energy&fuels

Article

pubs.acs.org/EF

Experimental and Modeling Study of Premixed Laminar Flames of Ethanol and Methane

Luc-Sy Tran, Pierre-Alexandre Glaude, René Fournet, and Frédérique Battin-Leclerc*

Laboratoire Réactions et Génie des Procédé, Université de Lorraine, CNRS, BP 20451, 1 Rue Grandville, 54001 Nancy, France

Supporting Information

ABSTRACT: To better understand the chemistry of the combustion of ethanol, the structure of five low pressure laminar premixed flames has been investigated: a pure methane flame (φ = 1), three pure ethanol flames (φ = 0.7, 1.0, and 1.3), and an ethanol/methane mixture flame (φ = 1). The flames have been stabilized on a burner at a pressure of 6.7 kPa using argon as a dilutant, with a gas velocity at the burner of 64.3 cm/s at 333 K. The results consist of mole fraction profiles of 20 species measured as a function of the height above the burner by probe sampling followed by online gas chromatography analyses. A mechanism for the oxidation of ethanol was proposed. The reactions of ethanol and acetaldehyde were updated and include recent theoretical calculations while that of ethenol, dimethyl ether, acetone, and propanal were added in the mechanism. This mechanism was also tested against experimental results available in the literature for laminar burning velocities and laminar premixed flame where ethenol was detected. The main reaction pathways of consumption of ethanol are analyzed. The effect of the branching ratios of reaction $C_2H_5OH + OH \rightarrow$ Products + H_2O is also discussed.

1. INTRODUCTION

As traditional fossil fuels are considered to be largely responsible for causing important atmospheric degradations, there is an increasing interest to shift from petroleum-based fuels to biofuels. The use of biofuels allows a reduction of the dependence on fossil fuels. Moreover, burning this renewable fuel should not lead to an increase of the total amount of greenhouse gases in the atmosphere. Many types of oxygenated molecules have been considered as potential additives to gasoline or diesel fuel, e.g., alcohols (methanol, ethanol, butanols...), fatty acid methyl esters, acyclic ethers (methyl *tert*-butyl ether (MTBE), ethyl *tert*-butyl ether (ETBE), dimethyl ether (DME)...), cyclic ethers of the family of furans (2-methylfuran, 2,5-dimethylfuran, 2-methyltetrahydrofuran, 2,5-dimethyltetrahydrofuran...).[1−4]

Ethanol has for several years been regarded as an attractive renewable alternative fuel with a high octane number (RON/MON = 120/99).[5] This oxygenated fuel can be obtained through the fermentation of sugars or starches which can be produced from very common crops, such as sugar cane or corn.[6] Recently ways to produce ethanol from cellulose[7] or algae[8] have also been proposed. Ethanol is now one of the most common and abundant biofuels.[9−11] Several previous studies have already been conducted to better understand each step of ethanol combustion and to develop oxidation mechanisms. Ethanol combustion has already been studied in static and flow reactors,[12,13,18] shock tubes,[14−16] rapid compression machines,[16] diffusion flames,[17] and laminar premixed flames.[18−22] Several kinetic studies on the combustion of the ethanol−hydrocarbon/gasoline fuel mixtures have been published.[21−26] A large number of studies of the laminar burning velocity of ethanol have been also published in recent years.[27−38] The first kinetic mechanisms proposed for the oxidation of this molecule, e.g. by Natarajan and Bhaskaran[39] and by Dunphy et al.,[40] were based on experimental data obtained in shock tubes. Norton and Dryer[41] published an oxidation mechanism which has been validated using experimental data obtained in a flow reactor. Dagaut et al.[42] proposed a kinetic reaction mechanism for ethanol pyrolysis and oxidation which has been validated using experimental data obtained with a flow tube, a jet-stirred reactor, and a shock tube. This mechanism has also been validated with ethanol−air flame speeds. Later, additional mechanisms have been developed by Marinov,[43] Saxena and Williams,[44] the team of Dryer,[13,45] Cancino et al.,[46] and Leplat et al.[18] All these mechanisms have been validated using experiments performed with several devices, including a laminar premixed flame.[18] Recently, Xu et al.[20] revised Zhao's dimethyl ether/ethanol mechanism[47] to model premixed laminar flames of dimethyl ether and ethanol at low pressure. The reactions involving ethenol (vinyl alcohol, C_2H_3OH), acetone, and ethyl methyl ether were included in this mechanism. Very recently, Lee et al.[16] proposed an updated model of the team of Dryer. This mechanism modeled the autoignition results obtained in a rapid compression machine and in a high temperature shock induced ignition delay. The results were also compared to the previously published low pressure, premixed flat flame molecular beam mass spectrometry speciation data of Kasper et al.[21] and Wang et al.[22]

Currently, the ethanol−methane mixture flame structure data are not available. Very little data is available for the formation of C_3 (non- and oxygenated) intermediates in ethanol flames. In addition, only the mechanism of Xu et al.[20] includes the reactions of ethenol to simulate the formation of this species in the ethanol flame. The objective of this study is to further improve the understanding of ethanol combustion by investigating experimentally the structure of five laminar premixed ethanol−methane flames at low pressure and to develop a model validating this new data and experimental data available in the literature.

Received: October 3, 2012
Revised: January 24, 2013

 © XXXX American Chemical Society dx.doi.org/10.1021/ef301628x | *Energy Fuels* XXXX, XXX, XXX−XXX

Table 1. Flame Inlet Conditions

flame name	φ[a]	initial mole fraction ethanol	CH_4	O_2	Ar	gas velocity at 333 K (cm/s)	dilution[c] (%)	mass flux (g cm^{-2} s^{-1})	C/O[a]	C/H[a]
pure methane flame	1.0	0.0000	0.0991	0.1989	0.7020	64.3	78	0.005 578	0.249	0.250
doped flame[b]	1.0	0.0207	0.0691	0.2008	0.7094	64.3	78	0.005 701	0.262	0.276
pure ethanol flame	1.0	0.0684	0.0000	0.2044	0.7272	64.3	78	0.005 991	0.287	0.333
	1.3	0.0870	0.0000	0.2006	0.7124	64.3	78	0.006 023	0.356	0.333
	0.7	0.0488	0.0000	0.2093	0.7419	64.3	78	0.005 972	0.209	0.333

[a]φ, equivalence ratio; C/O, carbon/oxygen ratio; C/H, carbon/hydrogen ratio. [b]Doped flame = ethanol/methane mixture flame. [c]Dilution = Ar/(Ar + O_2).

Table 2. Reactions of Dimethylether (CH_3OCH_3)[a]

reactions	A	n	E_a	references/notes	no.
$CH_3OCH_3 = CH_3O + CH_3$	9.44×10^{47}	−9.92	9.32×10^4	Zhao et al.[47,b]	D1
$CH_3OCH_3 + OH \Rightarrow CH_3 + HCHO + H_2O$	6.32×10^6	2.00	-0.65×10^3	De Vies et al.[95]	D2
$CH_3OCH_3 + H \Rightarrow CH_3 + HCHO + H_2$	7.72×10^6	2.09	3.38×10^3	De Vies et al.[95]	D3
$CH_3OCH_3 + O \Rightarrow CH_3 + HCHO + OH$	7.75×10^8	1.36	2.25×10^3	De Vies et al.[95]	D4

[a]The rate constants are given ($k = AT^n \exp(-E_a/RT)$) in cm^3, mol, s, cal units. [b]Rate constant taken from Zhao el al.[47] at 10.1 kPa (76 Torr). For other pressures (10^{-7}−10^4 kPa), the rate constants are given in the complete mechanism in Supporting Information 1.

2. EXPERIMENTAL METHODOLOGY

The experimental setup has been developed in our laboratory to study temperature and stable species profiles in a laminar premixed flat flame at low pressure and has been described previously.[50] Briefly, all flames were stabilized on a McKenna burner (diameter 60 mm, water-cooled) housed in a vacuum chamber which is maintained at 50 Torr (6.7 kPa) and equipped with a quartz probe with a hole of 180 μm diameter at the tip for sampling. The probe has an outer diameter of 6 mm and is tipped by a small cone with an angle to the vertical of 22° (its structure is presented in Supporting Information 3). The burner is cooled with water at a constant temperature of 333 K.

Methane (99.95% pure) was supplied by Alphagaz-Air Liquide, and oxygen (99.5% pure) and argon (99.995% pure) were provided by Messer. Liquid ethanol (>99.5% pure) was supplied by Sigma-Aldrich. Liquid ethanol was contained in a metallic vessel pressurized with argon. After each load of liquid fuel, argon bubbling and vacuum pumping were performed in order to remove oxygen traces dissolved in ethanol. Liquid ethanol was mixed with argon and then evaporated by passing it through a controlled evaporator and mixer (CEM). The temperature of this CEM was set at 373 K. Liquid and gas flow rates were measured by using mass flow controllers provided by BronKhorst, with a mass flow accuracy of ±0.5%.

Analyses were made using a gas chromatograph (GC) with a heated online connection to the probe, three types of columns (Carbosphere, HP-Plot Q, and HP-Molsieve) and two types of detectors (a flame ionization detector (FID) coupled with a methanizer and a thermal conductivity detector (TCD)). Stable species were identified by the determination of their individual retention times and by mass spectrometry (GC/MS). GC was calibrated directly using a cold-gas mixture for all species in the present GC measurement. The calculated uncertainties of the mole fraction measurements of the quantified species were about ± 5% for the major compounds, and ± 10% for minor products (<100 ppm). The FID detection threshold was about 1 ppm, while the TCD detection limit was about 50 ppm for H_2O, H_2, and O_2.

Flame temperature profiles were obtained using a PtRh (6%)-PtRh (30%) type B thermocouple (diameter 100 and 105 μm without and with an anticatalytic protective layer, respectively). The thermocouple wire was supported by an arm and crossed the flame horizontally to avoid conduction heat losses. The thermocouple junction was located at the center of the burner. The thermocouple was coated with an inert layer of BeO−Y_2O_3 to prevent catalytic effects when placed in a flame.[51] The ceramic layer was obtained by dipping the thermocouple in a hot solution of $Y_2(CO_3)_3$ (93% mass) and BeO (7% mass) followed by drying in a Meker burner flame. This process was repeated about 10 times until the whole metal was covered. Radiative heat losses were corrected using the electrical compensation method.[52] Uncertainty on the measurement of temperature was about ±100 K in the burned gases. In the fresh gases, there was an uncertainty of ±0.05 mm on the position of the temperature profile in the direction perpendicular to the burner surface. A sighting telescope (cathetometer) measured the position of the burner relative to the probe or the thermocouple with an accuracy of 0.01 mm.

Five flames were investigated in the present study: a pure methane flame (φ = 1), three pure ethanol flames (φ = 0.7, 1.0, and 1.3), and an ethanol−methane mixture flame (φ = 1). Dilution (78%), gas velocity (64.3 cm s^{-1} at 333 K), and pressure (6.7 kPa) have been kept the same for all flames. Additionally, the equivalence ratio has been kept the same at φ = 1 for the pure methane flame, the doped flame, and a pure ethanol (φ = 1) flame. The initial operating conditions of these flames are presented in Table 1.

3. ETHANOL KINETIC MODEL

A detailed kinetic mechanism was written in order to simulate experimental data concerning ethanol combustion. The mechanism proposed here to model the oxidation of ethanol includes two parts: (i) a reaction base used previously for C_0-C_4 species[53−55] and (ii) the mechanism proposed for the oxidation of ethanol. The complete mechanism involves 87 species in 760 reactions and is available in Supporting Information 1 under CHEMKIN format, together with the transport data file.

3.1. C_0-C_4 Reaction Database. This database has been comprehensively described in the previous papers.[50,55] The C_0-C_2 comprehensive submechanism includes all the unimolecular or bimolecular reactions involving radicals or molecules including carbon, hydrogen, and oxygen atoms and containing less than three carbon atoms. The C_3-C_4 reactions include reactions of unsaturated species, such as C_3H_2, C_3H_3, C_3H_4 (allene and propyne), C_3H_5, C_3H_6, C_3H_8, C_4H_2, C_4H_3, C_4H_4, C_4H_5, C_4H_6 (1,3-butadiene, 1,2-butadiene, 1-butyne, and 2-butyne), C_4H_7 (six isomers). This base contains also the reactions of acetone and propanal. In the present study, the reactions of formation and consumption of dimethylether (DME) have been added in order to simulate the mole fraction profile of DME detected in the present flames. Their kinetic parameters are listed in Table 2. The rate constant for the reaction D1 has been taken from Zhao el al.[47] at 10.1 kPa (76 Torr). For other pressures (10^{-7}−10^4 kPa), the rate constants of reaction D1 are given in the complete mechanism in Supporting Information 1.

dx.doi.org/10.1021/ef301628x | Energy Fuels XXXX, XXX, XXX−XXX

The rate constants of the reactions D2−D4 were taken from De Vies et al.[95] In these reaction bases, pressure-dependent rate constants follow the formalism proposed by Troe[58] and efficiency coefficients have been included.

3.2. Submechanism for the Oxidation of Ethanol. Table 3 presents the reactions of ethanol and derived species. This submechanism was built by reviewing the literature and by estimating rate constants which were not available.

3.2.1. Primary Mechanism. The primary mechanism contains the reactions of ethanol and of the radicals directly produced by them (reactions 1−52). Six channels of unimolecular decomposition reaction of ethanol (reactions 1−6) have been considered. These six reactions depend strongly on pressure. The kinetic parameters proposed by Tsang[60] were used for three reactions of ethanol (reactions 1−3), giving (C_2H_4 + H_2O) by pericyclic elimination, (CH_3 + CH_2OH) by C−C bond cleavage, or (C_2H_5 + OH) by C−O bond cleavage. Tsang[60] showed that the elimination of water (reaction 2) is the most significant reaction and is almost completely unaffected by the presence of the upper two bond breaking channels. The kinetic parameters recently estimated theoretically by the team of Lin[61] were used for reactions 4−6, giving (CH_2CH_2OH + H) or (CH_3CHOH + H) or (CH_3CH_2O + H) by C−H bond cleavage.

The kinetic parameters of the bimolecular initiations of ethanol with oxygen molecules (reactions 7−9), leading to the formation of three isomers of C_2H_5O radicals, ethoxy (CH_3CH_2O), α-hydroxyethyl (CH_3CHOH), β-hydroxyethyl (CH_2CH_2OH) radicals, have been obtained using the correlation proposed by Ingham et al.[62]

The H-abstractions from ethanol by flame propagating radicals (OH, H, CH_3, O, OOH, C_2H_5, CH_2OH, CH_3O) (reactions 10−30) involve the formation of CH_3CH_2O, CH_3CHOH, and CH_2CH_2OH radicals. The kinetic parameters of reactions 10, 11, 22, and 23 were deduced from the Evans−Polanyi plot proposed by Dean and Bozzelli[63] with ethane as a reference. A discussion about the effect on simulated results of the reaction C_2H_5OH + OH → Products + H_2O ($R_{EtOH+OH}$) including the three reactions 10−12 is presented in section 5.5. The rate constants for the reactions 12−21 have been obtained from the experimental and theoretical studies of the team of Lin[64−67] in the temperature range of 200−3000 K. The rate constants of the reactions 25, 26, 28, 29, and 30 were taken from the ethanol mechanism developed by Konnov et al.[68] The kinetic parameters for the H-atom abstraction from the alcohol functional group (reactions 24 and 27) have been obtained from the assumption of Grana et al.[69]

The three isomers of C_2H_5O radicals play a key role as reaction intermediates in the decomposition and combustion of ethanol.[39] The reactions of these radicals (reactions 31−52) include decompositions by β-scission (reactions 31, 32, 35, 36, 46, and 47), isomerization (reaction 33), isomerization-decompositions (reaction 37), oxidations (reactions 34, 38, 39, and 48), radical−radical disproportionations (reactions 40, 42, 44, 45, 49, 50, and 52), combinations with H-atom (reactions 43 and 51), and combination-decomposition (reaction 41). Rate parameters used for these reactions are those calculated by the team of Lin[61,70] in the temperature range of 200−3000 K, except for reactions 33, 38, 39, 44, 45, 48, 49, and 52. For the reaction 33, the pre-exponential factor of that in Konnov's mechanism[68] and the activation energy was deduced from the maximum energy barrier calculation of the team of Lin[70] was used. For reactions 38 and 39, the calculations of Da Silva et al.[71] at 10.1 kPa (76 Torr) were used. The parameters used in the Konnov's mechanism[68] were used for the reactions 44, 45, and 52. For the reactions 48 and 49, the estimation of Baulch et al.[56] and Marinov[43] were used, respectively.

Enols have been first postulated in 1880 by Erlenmeyer[94] as transient chemical intermediates in equilibrium with ketone or aldehyde through the keto−enol tautomerism. Ethenol (vinyl alcohol, C_2H_3OH), the simplest enol, was directly detected by Blank and Fischer[97] in 1973 and was observed in the gas phase by microwave spectroscopy by Saito[98] in 1976. Recently, enols have been detected as intermediate species in hydrocarbons and oxygenated fuel flames by photoionization molecular beam mass spectrometry (PI-MBMS).[20,48,72,73] Cool et al.[73] in 2003 observed the formation of ethenol in a rich ethylene flame. Ethenol, propenols, and butenols were reported in a wide range of pure and mixed-fuel flames by Taatjes et al.[72] in 2005. They discovered that, in the case of ethenol, the concentrations were far too high to be explained by the isomerization of acetaldehyde. The authors proposed that there should be a different mechanism in the formation of ethenol and acetaldehyde tautomers and that the flame concentrations are the result of the competing effects of many reactions. Taatjes et al.[48] in 2006 reported the mole fraction profiles of enols in the flames of ethene, allene, propene, butylenes, cyclopentene, and ethanol. They proposed that the reaction of OH radical with ethene (C_2H_4) is the dominant source of ethenol in many hydrocarbon flames as well as in ethanol flames. However, no modeling result was provided for the ethenol profile in the ethanol flame. Most recently, Xu et al.[20] detected ethenol in a stoichiometric pure ethanol flame. The ethenol formation pathway from OH addition to ethylene (C_2H_4) has been included in their model. However, this model underpredicted the formation of ethenol. In 2009, the theoretical studies of Xu et al.[70] and DaSilva et al.[71] have shown that ethenol can be formed from CH_2CH_2OH and CH_3CHOH radicals which are directly derived from ethanol by H-abstractions. However, these ethenol formation pathways were not included in most ethanol mechanisms reported in the literature. In our work, the formation of ethenol from CH_2CH_2OH and CH_3CHOH radicals has been added. The decompositions by β-scission of CH_2CH_2OH and CH_3CHOH radicals can lead to the formation of ethenol (reactions 32, 36) with a maximum barrier of about 33.4 kcal mol^{-1} and 33.8 kcal mol^{-1}, respectively.[70] The rate constants for these two reactions (32, 36) have been deduced from the theoretical calculations of the team of Lin[70] in the temperature range of 300−3000 K. These two reactions are strongly pressure-dependent, especially at high temperatures.[70] The oxidations (H-abstraction on radicals by O_2) of CH_2CH_2OH and CH_3CHOH radicals can also involve the formation of ethenol (reactions 34, 39). The rate constant of reaction 34 has been obtained using the correlation proposed by Buda el al.[74] for alkyl radicals, while that of reaction 39 had been obtained from the theoretical calculations of Da Silva et al.[71] in the temperature range of 200−3000 K. The reaction of CH_3CHOH radical with H atom (reaction 42) can also form ethenol via a transition state with a barrier of 0.8 kcal mol^{-1}. The rate constant for this reaction had been taken from the theoretical calculations of the team of Lin[61] in the temperature range of 100−2000 K.

3.2.2. Secondary Mechanism. The reactions involved in the primary mechanism of ethanol oxidation lead to the formation of the products, acetaldehyde (CH_3CHO), formaldehyde (HCHO), ethenol (C_2H_3OH), and ethylene (C_2H_4). The secondary mechanism includes the reactions of these primary products.

The reactions of formaldehyde and ethylene are included in the C_0-C_2 reactions database described above. There was no

dx.doi.org/10.1021/ef301628x | Energy Fuels XXXX, XXX, XXX−XXX

Table 3. Reactions of Ethanol and Derived Species[a]

reactions	A	n	E_a	refs/notes	no.
Primary mechanism:					
Reactions of ethanol (C_2H_5OH)					
$C_2H_5OH(+M) = C_2H_5 + OH(+M)$	2.95×10^{22}	−2.2	9.66×10^4	Tsang[60]	1
low pressure limit:	3.80×10^{88}	−19.7	1.15×10^{05}		
TROE centering: 0.209 40 × 10^1 0.165 39 × 10^5 0.111 40 × 10^1 0.161 36 × 10^3					
$C_2H_5OH(+M) = C_2H_4 + H_2O(+M)$	4.90×10^9	1.4	6.58×10^4	Tsang[60]	2
low pressure limit:	2.40×10^{80}	−17.9	8.48×10^4		
TROE centering: 0.212 60 × 10^1 0.135 68 × 10^5 0.969 00 × 10^0 0.160 40 × 10^3					
$C_2H_5OH(+M) = CH_3 + CH_2OH(+M)$	6.61×10^{23}	−2.2	8.80×10^4	Tsang[60]	3
low pressure limit:	1.99×10^{85}	−18.9	1.05×10^5		
TROE centering: 0.205 80 × 10^1 0.169 11 × 10^5 0.107 10 × 10^1 0.135 30 × 10^3					
$C_2H_5OH(+M) = CH_2CH_2OH + H(+M)$	2.01×10^{17}	−0.10	1.02×10^5	Xu et al.[61]	4
low pressure limit:	4.90×10^{94}	−21.65	1.23×10^5		
$C_2H_5OH(+M) = CH_3CHOH + H(+M)$	7.54×10^{16}	−0.30	9.40×10^4	Xu et al.[61]	5
low pressure limit:	7.71×10^{96}	−22.47	1.17×10^5		
$C_2H_5OH(+M) = CH_3CH_2O + H(+M)$	2.70×10^{15}	0.30	1.01×10^5	Xu et al.[61]	6
low pressure limit:	2.79×10^{88}	−19.76	1.21×10^5		
$C_2H_5OH + O_2 = CH_2CH_2OH + OOH$	2.10×10^{13}	0.00	5.24×10^4	estimation[b]	7
$C_2H_5OH + O_2 = CH_3CHOH + OOH$	1.40×10^{13}	0.00	4.63×10^4	estimation[b]	8
$C_2H_5OH + O_2 = CH_3CH_2O + OOH$	7.00×10^{12}	0.00	5.57×10^4	estimation[b]	9
$C_2H_5OH + OH = CH_3CHOH + H_2O$	2.40×10^6	2.00	-2.10×10^3	estimation[c]	10
$C_2H_5OH + OH = CH_2CH_2OH + H_2O$	3.60×10^6	2.00	9.50×10^2	estimation[c]	11
$C_2H_5OH + OH = CH_3CH_2O + H_2O$	2.81×10^2	3.00	-5.80×10^2	Xu and Lin[64]	12
$C_2H_5OH + O = CH_2CH_2OH + OH$	9.69×10^2	3.20	4.66×10^3	Wu et al.[65]	13
$C_2H_5OH + O = CH_3CHOH + OH$	1.45×10^5	2.50	8.76×10^2	Wu et al.[65]	14
$C_2H_5OH + O = CH_3CH_2O + OH$	1.46×10^{-3}	4.70	1.73×10^3	Wu et al.[65]	15
$C_2H_5OH + H = CH_2CH_2OH + H_2$	1.88×10^3	3.20	7.15×10^3	Park et al.[66]	16
$C_2H_5OH + H = CH_3CHOH + H_2$	1.79×10^5	2.50	3.42×10^3	Park et al.[66]	17
$C_2H_5OH + H = CH_3CH_2O + H_2$	5.33×10^{-23}	10.60	-4.46×10^3	Park et al.[66]	18
$C_2H_5OH + CH_3 = CH_2CH_2OH + CH_4$	3.30×10^2	3.30	1.23×10^4	Xu et al.[67]	19
$C_2H_5OH + CH_3 = CH_3CHOH + CH_4$	1.99×10^1	3.40	7.64×10^3	Xu et al.[67]	20
$C_2H_5OH + CH_3 = CH_3CH_2O + CH_4$	2.04×10^0	3.60	7.72×10^3	Xu et al.[67]	21
$C_2H_5OH + OOH = CH_2CH_2OH + H_2O_2$	4.20×10^4	2.70	1.91×10^4	estimation[c]	22
$C_2H_5OH + OOH = CH_3CHOH + H_2O_2$	2.80×10^4	2.70	1.54×10^4	estimation[c]	23
$C_2H_5OH + OOH = CH_3CH_2O + H_2O_2$	5.40×10^4	2.00	1.50×10^4	Grana et al.[69]	24
$C_2H_5OH + C_2H_5 = CH_2CH_2OH + C_2H_6$	1.50×10^{12}	0.00	1.17×10^4	Konnov et al.[68]	25
$C_2H_5OH + C_2H_5 = CH_3CHOH + C_2H_6$	4.00×10^{13}	0.00	1.00×10^4	Konnov et al.[68]	26
$C_2H_5OH + C_2H_5 = CH_3CH_2O + C_2H_6$	2.30×10^4	2.00	1.05×10^4	Grana et al.[69]	27
$C_2H_5OH + CH_2OH = CH_3CHOH + CH_3OH$	4.00×10^{11}	0.00	9.70×10^3	Konnov et al.[68]	28
$C_2H_5OH + CH_3O = CH_3CHOH + CH_3OH$	2.00×10^{11}	0.00	7.00×10^3	Konnov et al.[68]	29
$C_2H_5OH + CH_3CH_2O = C_2H_5OH + CH_3CHOH$	2.00×10^{11}	0.00	7.00×10^3	Konnov et al.[68]	30
Reactions of CH_2CH_2OH radicals					
$CH_2CH_2OH = C_2H_4 + OH$	3.52×10^{-34}	11.80	-1.87×10^4	Xu et al.[70]	31
$CH_2CH_2OH = H + C_2H_3OH$	3.33×10^{28}	−5.30	3.56×10^4	Xu et al.[70]	32
$CH_2CH_2OH = CH_3CHOH$	1.00×10^{11}	0.00	3.95×10^4	Xu et al.[70,d]	33
$CH_2CH_2OH + O_2 = C_2H_3OH + OOH$	1.60×10^{12}	0.00	5.00×10^3	estimation[e]	34
Reactions of CH_3CHOH radicals					
$CH_3CHOH = CH_3CHO + H$	8.34×10^{27}	−5.20	3.56×10^4	Xu et al.[70]	35
$CH_3CHOH = H + C_2H_3OH$	2.00×10^{28}	−5.10	3.94×10^4	Xu et al.[70]	36
$CH_3CHOH = CH_3 + HCHO$	1.14×10^{22}	−3.60	3.47×10^4	Xu et al.[70]	37
$CH_3CHOH + O_2 = CH_3CHO + OOH$	5.26×10^{17}	−1.60	8.38×10^2	DaSilva et al.[71]	38
$CH_3CHOH + O_2 = C_2H_3OH + OOH$	5.33×10^2	2.50	-4.02×10^2	DaSilva et al.[71]	39
$CH_3CHOH + H = CH_3CHO + H_2$	1.36×10^9	1.30	2.82×10^3	Xu et al.[61]	40
$CH_3CHOH + H = CH_2OH + CH_3$	8.67×10^{16}	−0.90	2.90×10^3	Xu et al.[61]	41
$CH_3CHOH + H = C_2H_3OH + H_2$	4.90×10^8	1.70	5.88×10^2	Xu et al.[61]	42

dx.doi.org/10.1021/ef301628x | Energy Fuels XXXX, XXX, XXX−XXX

Table 3. continued

reactions	A	n	E_a	refs/notes	no.
$CH_3CHOH + H(+M) = C_2H_5OH(+M)$	3.61×10^{13}	0.10	4.37×10^{2}	Xu et al.[61]	43
low pressure limit:	2.77×10^{56}	−15.72	1.07×10^{4}		
$CH_3CHOH + OH = CH_3CHO + H_2O$	1.50×10^{13}	0.00	0.00×10^{0}	Konnov et al.[68]	44
$CH_3CHOH + O = CH_3CHO + OH$	9.04×10^{13}	0.00	0.00×10^{0}	Konnov et al.[68]	45
Reactions of CH_3CH_2O radicals					
$CH_3CH_2O = CH_3 + HCHO$	4.40×10^{-29}	10.70	-1.62×10^{4}	Xu et al.[70]	46
$CH_3CH_2O = H + CH_3CHO$	4.25×10^{-32}	11.50	-1.65×10^{4}	Xu et al.[70]	47
$CH_3CH_2O + O_2 = CH_3CHO + OOH$	6.00×10^{10}	0.00	1.70×10^{3}	Baulch et al.[56]	48
$CH_3CH_2O + OH = CH_3CHO + H_2O$	1.00×10^{13}	0.00	0.00×10^{0}	Marinov[43]	49
$CH_3CH_2O + H = CH_3CHO + H_2$	7.47×10^{9}	1.10	6.74×10^{2}	Xu et al.[61]	50
$CH_3CH_2O + H(+M) = C_2H_5OH(+M)$	3.08×10^{11}	0.90	1.29×10^{1}	Xu et al.[61]	51
low pressure limit:	3.77×10^{51}	−15.55	1.11×10^{4}		
$CH_3CH_2O + O = CH_3CHO + OH$	1.21×10^{14}	0.00	0.00×10^{0}	Konnov et al.[68]	52
Secondary mechanism:					
Reactions of ethenol (C_2H_3OH)					
$C_2H_3OH + O = CH_2CHO + OH$	1.40×10^{13}	0.00	2.30×10^{3}	estimation[f]	53
$C_2H_3OH + H = CH_2CHO + H_2$	1.31×10^{5}	2.60	1.22×10^{3}	estimation[f]	54
$C_2H_3OH + OH = CH_2CHO + H_2O$	2.30×10^{10}	0.73	-1.10×10^{3}	estimation[f]	55
$C_2H_3OH + OOH = CH_2CHO + H_2O_2$	1.00×10^{12}	0.00	1.00×10^{4}	estimation[f]	56
$C_2H_3OH + CH_3 = CH_2CHO + CH_4$	2.00×10^{-06}	5.60	2.50×10^{3}	estimation[f]	57
$C_2H_3OH + C_2H_5 = CH_2CHO + C_2H_6$	1.30×10^{12}	0.00	8.50×10^{3}	estimation[f]	58
$C_2H_3OH = CH_3CHO$	4.50×10^{06}	1.80	5.10×10^{4}	calculation[g]	59
$C_2H_3OH + H = CH_3CHO + H$	1.00×10^{13}	0.00	1.51×10^{3}	estimation[h]	60
$C_2H_3OH + OH = CH_3 + CO_2 + H_2$	1.40×10^{12}	0.00	-1.04×10^{3}	estimation[i]	61
$C_2H_4 + OH = C_2H_3OH + H$	4.00×10^{12}	0.00	4.88×10^{3}	Hippler and Viskolcz[80]	62
Reactions of acetaldehyde (CH_3CHO)					
$CH_3CHO + OH = CH_3CO + H_2O$	2.30×10^{10}	0.70	-1.10×10^{3}	Konnov et al.[68]	63
$CH_3CHO + OH = CH_2CHO + H_2O$	3.37×10^{11}	0.0	-0.62×10^{3}	San Diego Mechanism[96]	64
$CH_3CHO + H = H_2 + CH_3CO$	1.31×10^{05}	2.60	1.22×10^{3}	Sivaramakrishnan et al.[90]	65
$CH_3CHO + H = CH_2CHO + H_2$	2.72×10^{03}	3.1	5.21×10^{3}	Sivaramakrishnan et al.[90]	66
$CH_3CHO + CH_3 = CH_3CO + CH_4$	2.00×10^{-06}	5.60	2.50×10^{3}	Baulch et al.[56]	67
$CH_3CHO + CH_3 = CH_2CHO + CH_4$	2.45×10^{01}	3.15	5.73×10^{3}	Marinov[43]	68
$CH_3CHO + O = CH_3CO + OH$	1.40×10^{13}	0.00	2.30×10^{3}	Cavanagh and Cox[91]	69
$CH_3CHO + O = CH_2CHO + OH$	3.72×10^{13}	−0.2	3.56×10^{3}	Marinov[43]	70
$CH_3CHO + C_2H_3 = C_2H_4 + CH_3CO$	8.10×10^{10}	0.00	3.70×10^{3}	Scherzer et al.[92]	71
$CH_3CHO + C_2H_5 = C_2H_6 + CH_3CO$	1.30×10^{12}	0.00	8.50×10^{3}	Hohlein and Freeman[93]	72
$CH_3CHO + CH_3O = CH_3CO + CH_3OH$	5.00×10^{12}	0.00	0.00×10^{0}	Konnov et al.[68]	73
$CH_3CHO + CH_2CHO = CH_3CHO + CH_3CO$	3.00×10^{12}	0.00	1.12×10^{4}	Konnov et al.[68]	74
$CH_3CHO + OOH = CH_3CO + H_2O_2$	1.00×10^{12}	0.00	1.00×10^{4}	Cavanagh and Cox[91]	75
$CH_3CHO + O_2 = CH_3CO + OOH$	5.00×10^{13}	0.00	3.64×10^{4}	Cavanagh and Cox[91]	76
$CHO + CH_3 = CH_3CHO$	1.80×10^{13}	0.00	0.00×10^{0}	Tsang and Hampson[57]	77
Reactions of formaldehyde (HCHO)	See them in complete mechanism in Supporting Information 1				
Reactions of ethylene (C_2H_4)	See them in complete mechanism in Supporting Information 1				

[a]The rate constants are given ($k = AT^n \exp(-E_a/RT)$) in cm^3, mol, s, cal units. [b]Rate constant estimated by using the correlation proposed by Ingham et al.[62] [c]Rate constant estimated by using the Evans−Polanyi plot proposed by Dean and Bozzelli.[63] [d]Pre-exponential factor obtained from Konnov's mechanism.[68] Activation energy obtained from the calculation of the team of Lin (Xu et al.).[70] [e]Rate constant estimated by using the correlation proposed by Buda et al.[74] for alkyl radicals. [f]Rate constant estimated by analogy with the values proposed for acetaldehyde. [g]Rate constant calculated by means of quantum calculations at the CBS-QB3 method[81] implemented in the Gaussian 03 program suite,[82] for a temperature range of 700−2000 K and high pressure limit. [h]Rate constant estimated by using that proposed by Warnatz[78] for the H addition to C_2H_4, with the assumption, proposed by Huynh et al.[77] that the leaving of the alcoholic hydrogen is instantaneous. [i]By analogy, the rate constant is that proposed by Wilk et al.[79] for the addition of OH radical on the double bond of propene.

modification for these reactions in this study. The reactions of acetaldehyde have been updated in order to improve simulations for the acetaldehyde profile. Their kinetic parameters are listed in Table 3 (reactions 63−77) and were obtained from a review of the literature.

In the mechanism of Xu et al.,[20] the rate constants of the H-abstractions from ethenol were estimated from that of methanol. Since very little data is available for ethenol reactions, the bond dissociation energies (BDE) in ethanol, ethenol, methanol, and acetaldehyde molecules were analyzed and compared (see Figure 1). Since the O−H bond in methanol is much stronger than in ethenol, we chose the rate constants of the H-abstractions from the carbonyl group (−CHO) of acetaldehyde (BDE = 88.8 kcal mol^{-1}) to represent those from the hydroxyl group (−OH) of

dx.doi.org/10.1021/ef301628x | Energy Fuels XXXX, XXX, XXX−XXX

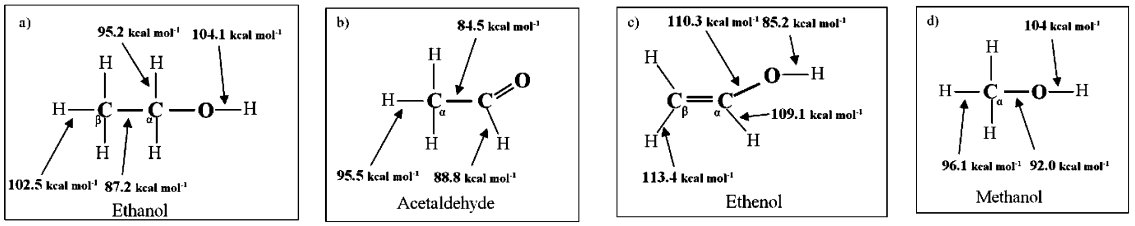

Figure 1. Bond dissociation energies in ethanol, ethenol, acetaldehyde, and methanol molecules.[71,75,76].

ethenol (BDE = 85.2 kcal mol^{-1}) (reactions 53−58). The rate constants for the unimolecular tautomerization from ethenol to acetaldehyde (reaction 59) had been determined by theoretical calculation in the temperature range of 700−2000 K (see the detailed calculation in following paragraph). The isomerization route catalyzed by H (reaction 60) is also included for the enol tautomerization. The rate constants of this reaction was estimated by using that proposed by Warnatz[78] for the H addition to C_2H_4, with the additional assumption, proposed by Huynh et al.,[77] that the leaving of the alcoholic hydrogen is instantaneous. Reaction 61 is an addition of the OH radical on the double bond of ethenol. We assumed that the addition of OH radical to ethenol leads to the formation of an adduct, which can decompose into CH_3, CO_2, and a H-atom. The rate constant is assumed to be analogous to that proposed by Wilk et al.[79] for the addition of a OH radical on the double bond of propene. The rate constant of reaction 62, the addition of H-atoms to ethenol, is that proposed by Hippler and Viskolcz.[80]

The concerted reaction of ethenol yielding acetaldehyde (reaction 59) was investigated by means of quantum calculations using the CBS-QB3 method[81] implemented in the Gaussian 03 program suite.[82] This method is commonly used to calculate accurate thermochemical data and energy barriers.[83] For close shell systems, a precision of 1.5 kcal mol^{-1} can be expected for energy calculations. Figure 2 depicts the

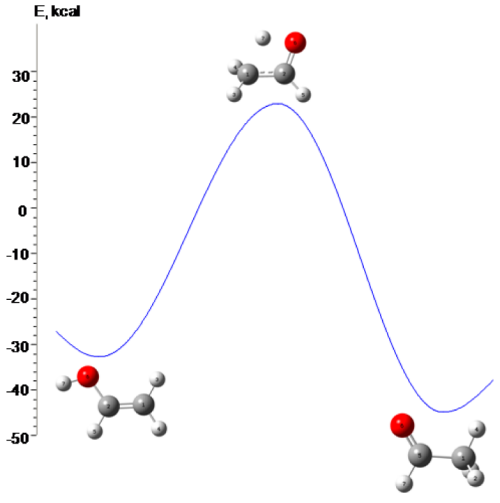

Figure 2. Isomerization of ethenol to acetaldehyde computed using the CBS-QB3 method at 0 K.

isomerization of ethenol to acetaldehyde with the calculated concerted transition state. At 0 K, the reaction is exothermic by −12 kcal mol^{-1} and the corrected energy barrier is estimated to be close to 56 kcal mol^{-1}, which is in agreement with the value of 54.73 kcal mol^{-1} obtained by Teixeira-Dias et al.[84] at the MP4/6-31++G(d,p) level of theory.

Canonical transition state theory implemented in the Chemrate software[85] was used to calculate the high pressure limit rate constant using eq1:

$$k_\infty(T) = \kappa L \frac{k_B T}{h} \frac{Q_{TS}(T)}{Q_R(T)} \exp\left[-\frac{V^\ddagger}{RT}\right] \quad (1)$$

where k_B is Boltzmann's constant, h is Planck's constant, T the temperature, and $V^\ddagger$ the classical barrier height. $Q_{TS}(T)$ and $Q_R(T)$ represent the partition function calculated, respectively, for the transition state (TS) and the reactant (R). κ is the transmission coefficient and has been estimated using the Eckart[86] approximation for reactions involving H-atom transfer. L is the statistical factor defined as

$$L = \frac{\sigma_R n_{TS}}{\sigma_{TS} n_R} \quad (2)$$

In eq2, σ_R and σ_{TS} are the external symmetry of the reactant and the transition state respectively, while n_R and n_{TS} correspond to their number of optical isomers. In the calculation of $k_\infty(T)$, σ_R and σ_{TS} were removed from the rotational partition function to avoid counting them twice. The vibrational partition function was calculated using the harmonic oscillator (HO) approximation, except for internal rotations which were treated as hindered rotations (HR) by means of the Pitzer and Gwinn approximation.[87] The rotational barriers associated to hindered rotations were calculated by performing a relaxed scan at the B3LYP/cbsb7 level of theory. However, for the transition state the reaction coordinate has been frozen which prevents any internal rotation.

Finally, the three parameter Arrhenius expression has been derived between 700 and 2000 K for the high pressure rate constant with the software Chemrate:[85]

$$k_\infty = 4.5 \times 10^6 T^{1.8} \exp\left(-\frac{51\,006}{RT}\right) \text{s}^{-1} \quad (3)$$

In equation (eq 3), E_a is in cal mol^{-1}, R in cal mol^{-1} K^{-1}, and T in K. Our value calculated at the CBS-QB3 level of theory fits well with the calculation of Da Silva et al.[76] at the CBS-APNO level of theory, with a ratio of 1.5 at 1200 K.

4. EXPERIMENTAL RESULTS

The carbon (C), hydrogen (H), and oxygen (O) balances were checked in all five flames. The quantified mole fraction of argon allowed one to take into account the change in the total mole number along the flame profiles. The difference between inlet and outlet is about 5% in the post flame region and 6% in the reaction zone for C, about 5% in the post flame region and 9% in the reaction zone for O, and about 5% in the post flame region and 10% in the reaction zone for H. In the following paragraphs, the flame temperature profiles and mole fraction profiles of

dx.doi.org/10.1021/ef301628x | Energy Fuels XXXX, XXX, XXX−XXX

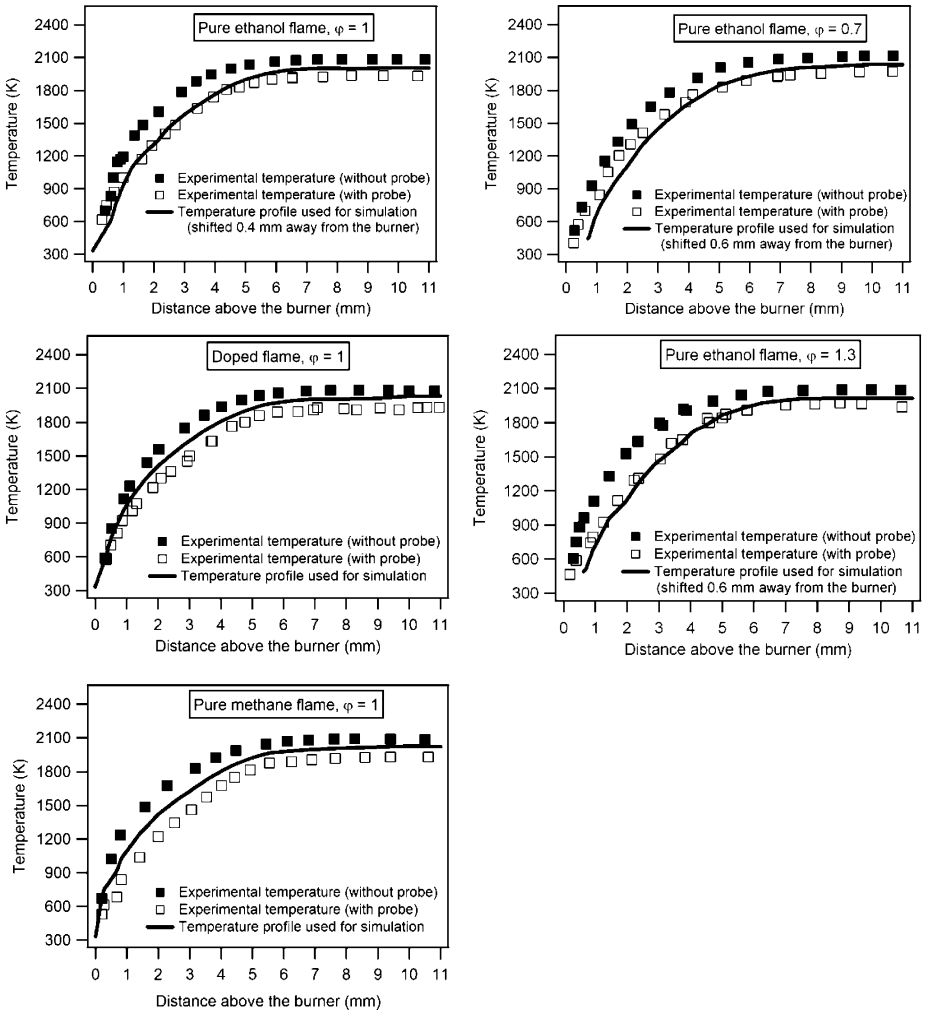

Figure 3. Flame temperature profiles for the five flames: experimental measurements performed without and with the sampling probe and profile used for simulation.

reactants, products, and intermediate species of the five flames are presented.

Figure 3 shows the temperature profiles measured for the five flames with and without the sampling probe and the profile used for simulation. The figure shows that the presence of the probe induces a thermal perturbation which causes a lower measured temperature. Without the probe, the lowest temperatures were around 700 K (at 0.4 mm height) in the stoichiometric pure ethanol flame, around 520 K (at 0.3 mm height) in the lean pure ethanol flame, around 600 K (at 0.3 mm height) in the rich pure ethanol flame, around 590 K (at 0.3 mm height) in the doped flame, and around 670 K (at 0.3 mm height) in the pure methane flame. Because of the size of the thermocouple, it was not possible to measure a temperature closer to the burner. The maximum temperature of around 2100 K in the post flame region was very similar for the five flames and was reached 6 mm above the burner.

Figures 4−14 present mole fraction profiles of several stable species as a function of the height above the burner for the five flames. It can be said that the mole fractions of most the identified intermediate products in the five flames have their maxima in the range of 1−3 mm from the burner surface.

Figures 4 and 5 present the profiles of reactants, including ethanol (C_2H_5OH), methane (CH_4), argon (Ar), and oxygen (O_2). Figure 4 shows that ethanol is completely consumed close to the burner, at a height of 2.5−2.8 mm, while some methane remains up to a height of 3.5 mm. The reason for this difference is that the laminar flame speed of methane/oxygen mixture is slower than that of the ethanol/oxygen mixture.[88] This implies that the pure methane flame front is further from the burner. For the stoichiometric and lean flames, there is a significant remaining mole fraction of O_2 (Figure 5) in the post flame region, but this is not the case for the rich flame.

Figures 6 and 7 present mole fraction profiles of the major products, including carbon dioxide (CO_2), water (H_2O), hydrogen (H_2), and carbon monoxide (CO). The major final products are, to a large extent, CO_2 and H_2O (Figure 6). Among the five flames, the mole fraction of CO_2 formed in stoichiometric pure ethanol flame is the largest (mole fraction of 0.087 at 8.0 mm height). The profiles of H_2 (Figure 7) display a marked maximum at a height of 2.5 mm in the stoichiometric pure ethanol flame and is at a height of 3.0 mm in the other flames. Among the five flames, the mole fraction of H_2 formed in the rich pure ethanol flame is the largest (mole fraction of 0.073 at height 3.0 mm). In the stoichiometric pure ethanol flame, the profile of CO (Figure 7) displays a marked maximum at a height of 2.8 mm but is at a height of 3.5 mm in the other flames. The maximum mole fraction of CO formed in the rich pure ethanol flame is the largest (mole fraction of 0.105 at height 3.5 mm). It can be seen from Figure 7 that there is a remaining mole fraction of CO and H_2 in the post flame region.

dx.doi.org/10.1021/ef301628x | *Energy Fuels* XXXX, XXX, XXX−XXX

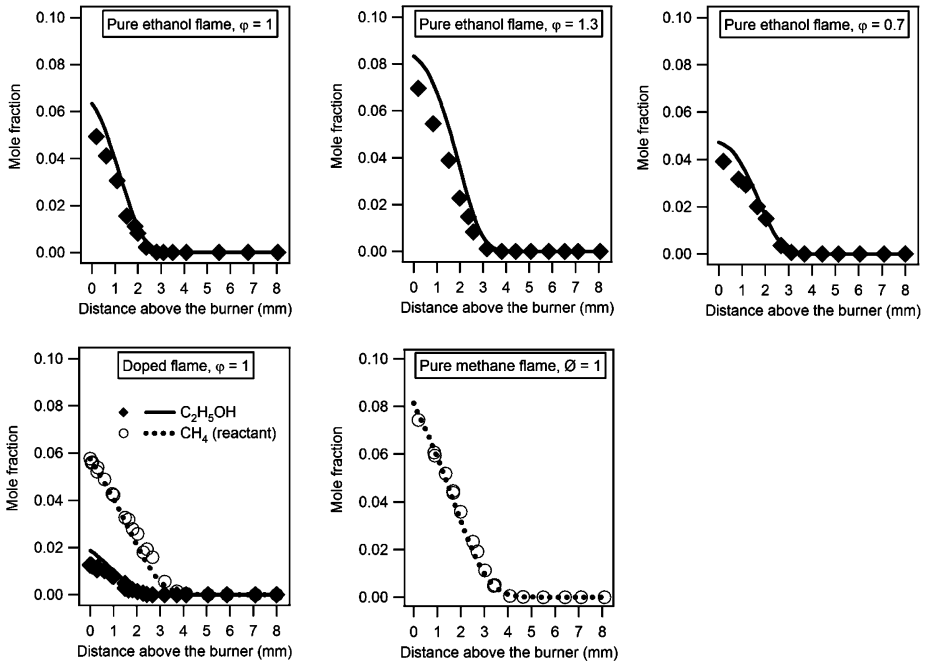

Figure 4. Mole fraction profiles of fuels: C_2H_5OH, CH_4 (reactant). Points are experiments and lines are simulations: filled diamonds and solid lines, C_2H_5OH; open circles and dotted lines, CH_4.

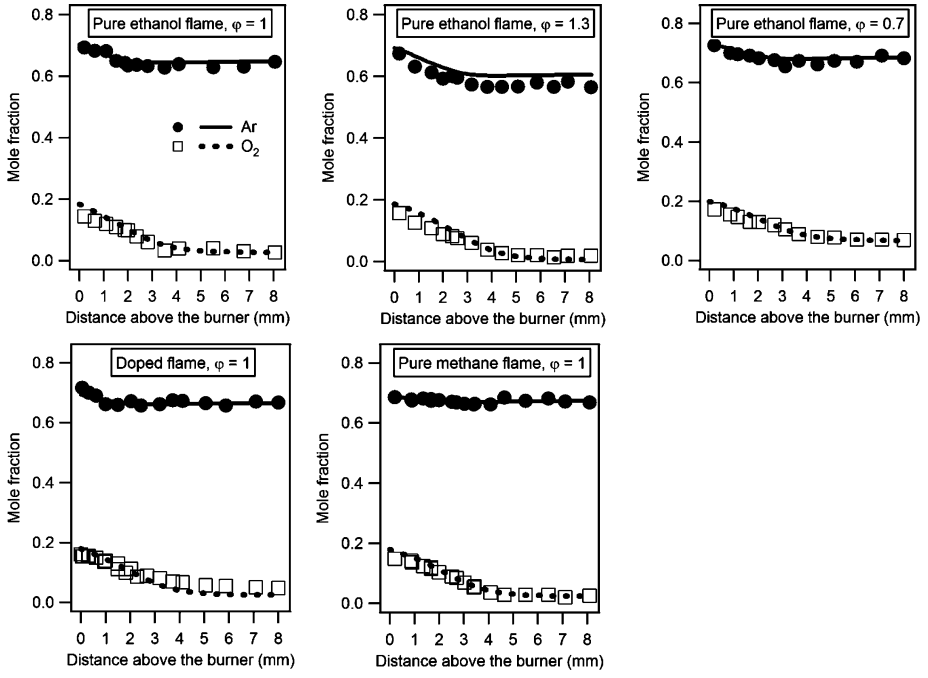

Figure 5. Mole fraction profiles of O_2 and Ar. Points are experiments and lines simulations: filled circle and solid lines, Ar; open squares and dotted lines, O_2.

The mole fraction profiles of the intermediate CH_4 are shown in Figure 8. In the stoichiometric pure ethanol flame, the profile of CH_4 displays a marked maximum at height 2.0 mm and is at 2.5 mm in the rich and lean pure ethanol flames. The mole fraction of CH_4 in the rich flame is the largest (4200 ppm at 2.5 mm height), followed by the stoichiometric ethanol flame (2670 ppm at 2.0 mm height), and finally the lean ethanol flame (1560 ppm at 2.5 mm height).

The mole fraction profiles of C_2 nonoxygenated intermediates, including ethane (C_2H_6), ethylene (C_2H_4), and acetylene (C_2H_2) are shown in Figure 9.

The mole fraction of C_2H_6 (Figure 9) in the rich flame is the largest (up to 1400 ppm), followed by the stoichiometric flames, and finally the lean flame. In the three stoichiometric flames, the highest mole fraction of C_2H_6 is very similar in both pure ethanol and pure methane flames and is slightly reinforced in the doped flame. In the stoichiometric pure ethanol flame, the profiles of C_2H_6 display a marked maximum at height 2.3 mm and is at 2.8 mm in the rich and lean pure ethanol flames, which is at 1.8 mm and 1.6 mm in the doped and pure methane flame, respectively. Among C_2 species in the pure methane flame, C_2H_6 is the most abundant and is produced first.

dx.doi.org/10.1021/ef301628x | *Energy Fuels* XXXX, XXX, XXX−XXX

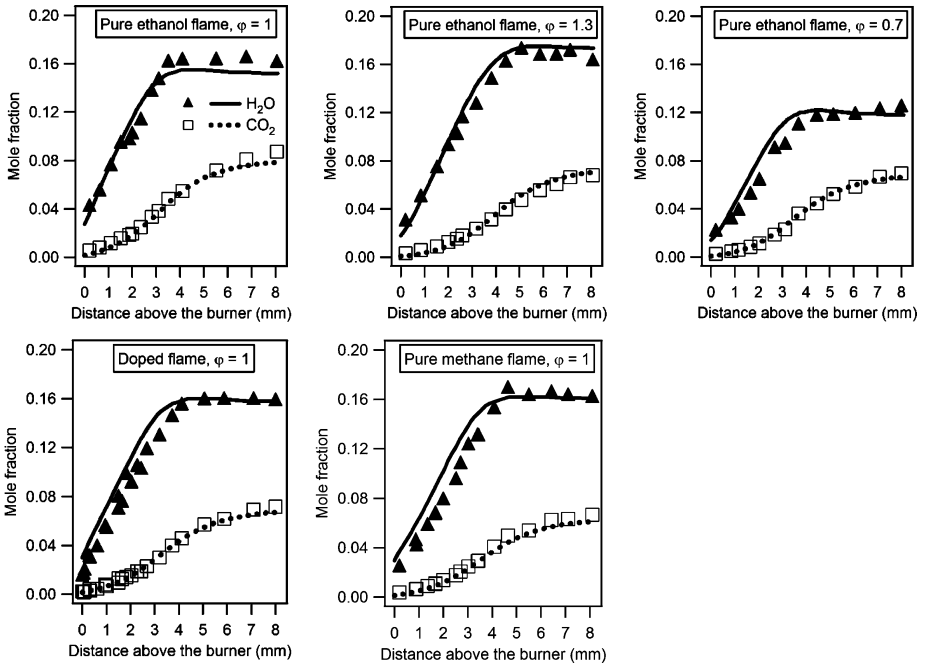

Figure 6. Mole fraction profiles of CO_2 and H_2O. Points are experiments and lines simulations: filled triangles and solid lines, H_2O; open squares and dotted lines, CO_2.

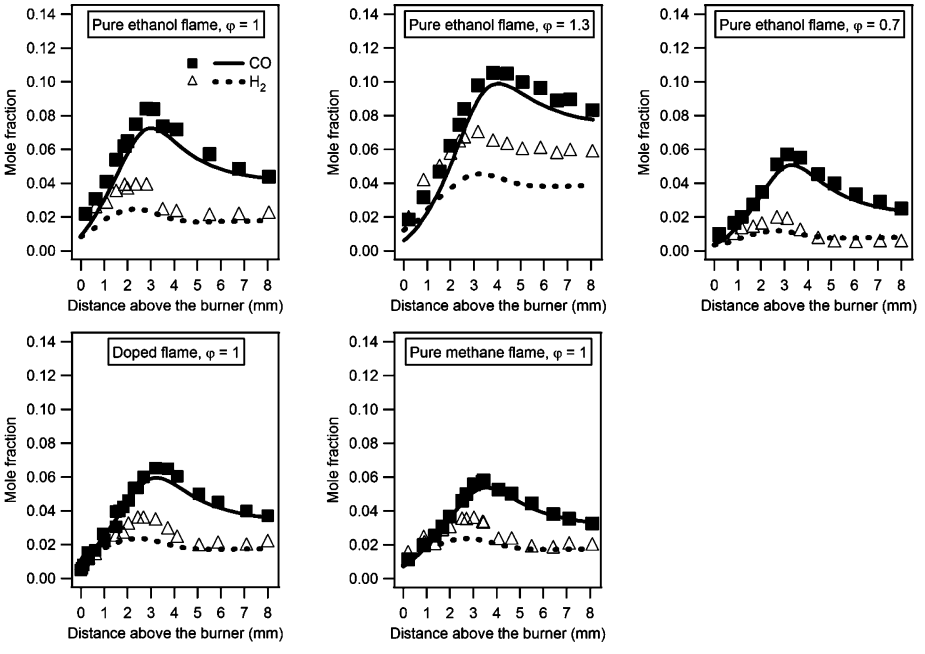

Figure 7. Mole fraction profiles of CO and H_2. Points are experiments and lines simulations: filled squares and solid lines, CO; open triangles and dotted lines, H_2.

The mole fraction of C_2H_4 (Figure 9) in the rich pure ethanol flame is the largest (peak mole fraction of 7500 ppm) and that in the pure methane flame is the lowest (peak mole fraction of 500 ppm). In the stoichiometric pure ethanol and doped flame, the profile of C_2H_4 displays a marked maximum at height 2.0 mm and is at 2.5 mm in the other flames. Among C_2 nonoxygenated species, in the pure ethanol and doped flames, C_2H_4 is the most abundant and is produced first.

The maximum mole fraction of C_2H_2 (Figure 9) is considerably increased in the doped flame (peak mole fraction of 450 ppm at 2.5 mm height) compared to the pure methane flame (peak mole fraction of 185 ppm at 2.8 mm height), and it even reaches a higher level in the rich and stoichiometric pure ethanol flames (peak mole fraction of 2660 ppm at height 3.0 mm, 1020 ppm at 2.5 mm height, respectively). C_2H_2 is considered to be the most representative soot precursor in a variety of hydrocarbon fuel flames because it yields benzene and aromatic rings, the first step toward the production of soot.[89]

Figures 10 and 11 present the profiles of the C_3 nonoxygenated intermediates, including propane (C_3H_8), propene (C_3H_6) (Figure 10), propyne (pC_3H_4), and allene (aC_3H_4) (Figure 11). These figures show that a very small amount of C_3 products is observed in the pure methane flame.

dx.doi.org/10.1021/ef301628x | *Energy Fuels* XXXX, XXX, XXX−XXX

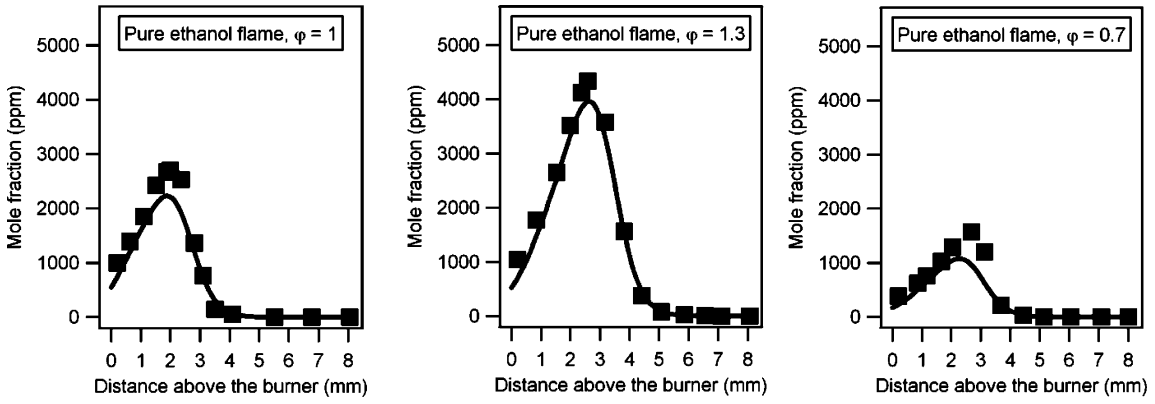

Figure 8. Mole fraction profiles of CH_4 (intermediate). Points are experiments and lines simulations: filled squares and solid lines, CH_4.

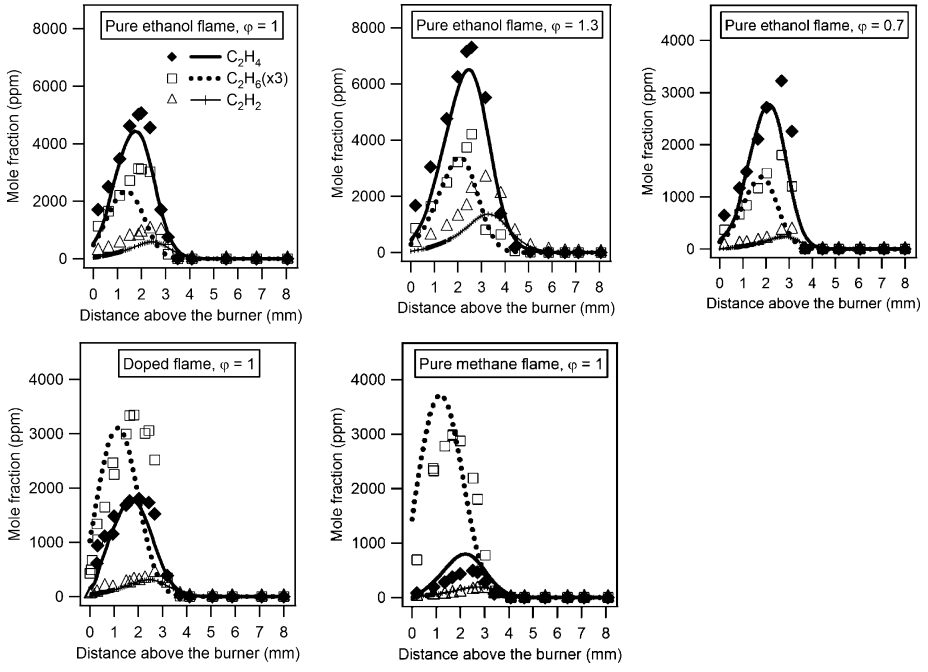

Figure 9. Mole fraction profiles of C_2H_6, C_2H_4, and C_2H_2. Points are experiments and lines simulations: filled diamonds and solid lines, C_2H_4; open squares and dotted lines, C_2H_6; open triangles and lines and markers, C_2H_2.

The mole fraction of C_3H_8 (Figure 10) in the rich pure ethanol flame is the largest (peak mole fraction of 73 ppm at height 2.5 mm), followed by the stoichiometric pure ethanol and doped flames (peak mole fraction of 64 ppm and 53 ppm at 2.0 mm height, respectively), and finally the pure methane and lean pure ethanol flames (peak mole fraction of 28 ppm at 1.8 mm height and 34 ppm at 2.7 mm height, respectively).

The peak mole fraction of C_3H_6 (Figure 10) is 105 ppm (at 2.0 mm height), 155 ppm (at 2.5 mm height), 48 ppm (at 2.5 mm height), 35 ppm (at 2.0 mm height), and 5 ppm (at 2.0 mm height) in the stoichiometric, rich, lean pure ethanol flames, doped, and pure methane flames, respectively.

Figure 11 displays the profiles of pC_3H_4 and aC_3H_4. In the rich pure ethanol flame, the mole fraction of pC_3H_4 and aC_3H_4 is the largest (about 17 ppm for pC_3H_4 and about 8 ppm for aC_3H_4) and is lower than the limit of detection of the gas chromatograph in the pure methane flame. The mole fraction of pC_3H_4 is higher than that of aC_3H_4 with a factor of about 2.

Figures 12−14 display the profiles of oxygenated species, formaldehyde (HCHO), acetaldehyde (CH_3CHO) (Figure 12), dimethylether (CH_3OCH_3) (Figure 13), acetone (CH_3COCH_3), and propanal (C_2H_5CHO) (Figure 14). HCHO and CH_3CHO (Figure 12) were quantified with a quite high mole fraction in the ethanol flames (about 1500−3000 ppm for HCHO and 2000−6000 ppm for CH_3CHO). The profiles of CH_3CHO and CH_3OCH_3 reach their maximum mole fractions close to the burner, around 1.0−1.8 mm height. The mole fraction of CH_3OCH_3 (Figure 13) in the stoichiometric and rich pure ethanol flames is the largest (about 30 ppm) followed by the lean and doped flames (about 20 ppm), and finally the pure methane flame (about 5 ppm). C_3 oxygenated species were also detected, CH_3COCH_3 and C_2H_5CHO (Figure 14), with a low mole fraction (about 10−30 ppm for C_2H_5CHO and 30−50 ppm for CH_3COCH_3). Acetaldehyde, acetone, and propanal were not detected in the pure methane flame. Ethenol (vinyl alcohol) is quite reactive. This does not allow one to be detected in our GC measurement. Note that, in the reports of the literature,[20,48,72,73] ethenol has been detected by PI-MBMS. The experimental data of our study are also given in tabular form in Supporting Information 2.

dx.doi.org/10.1021/ef301628x | *Energy Fuels* XXXX, XXX, XXX−XXX

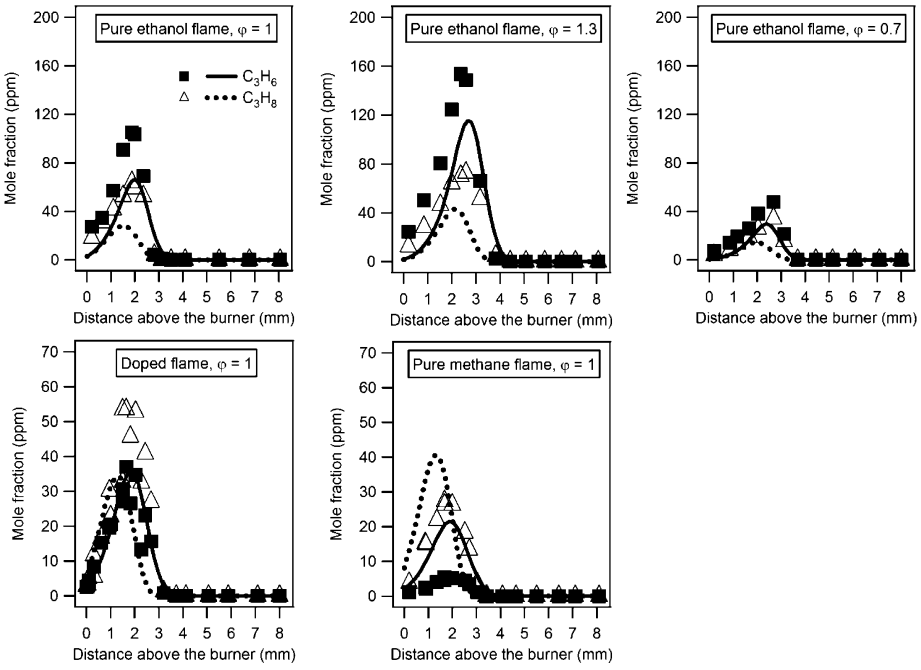

Figure 10. Mole fraction profiles of C_3H_8 and C_3H_6. Points are experiments and lines simulations: filled squares and solid lines, C_3H_6; open triangles and dotted lines, C_3H_8.

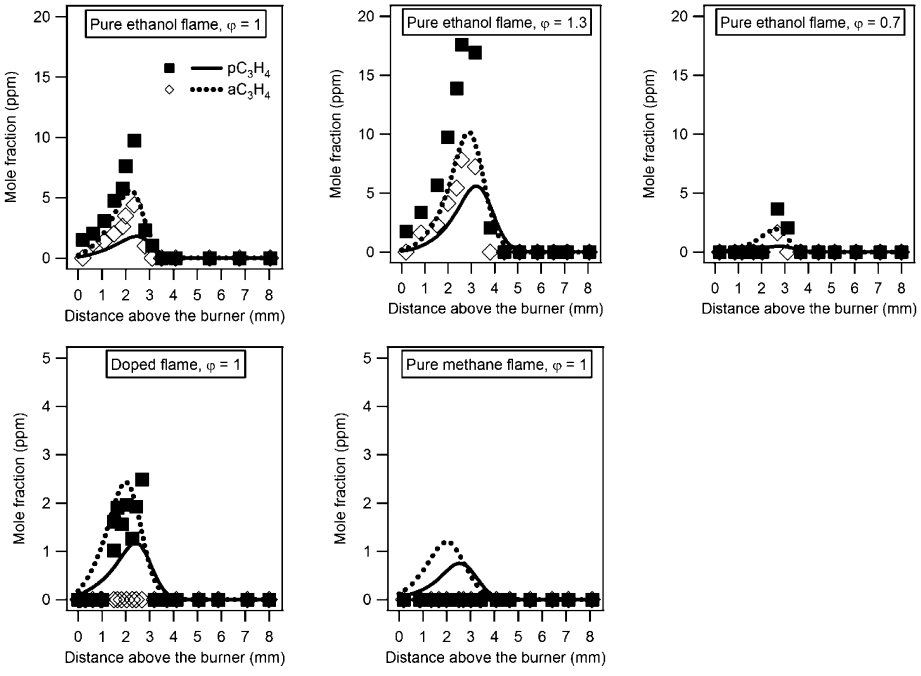

Figure 11. Mole fraction profiles of pC_3H_4 and aC_3H_4. Points are experiments and lines simulations: filled squares and solid lines, pC_3H_4; open diamonds and dotted lines, aC_3H_4.

5. COMPARISON BETWEEN EXPERIMENTAL AND SIMULATED RESULTS

5.1. Present Laminar Premixed Flames Results. Simulations were performed using PREMIX software from CHEMKIN[59] using the experimental temperature profile as an input. Thermal diffusion has been included. Convergence criteria were decreased until a grid independent solution was found. To compensate for the perturbations induced by the quartz probe and the thermocouple,[99−101] the temperature profile used in calculations is an average between the experimental profiles measured with and without the quartz probe, shifted away from the burner surface, in a height range of 0−0.6 mm, as shown in Figure 3. A deepened study about the influence of sampling probe on temperature profile and species concentration can be found in the studies of the team of Pr. Kohse-Höinghauss[99,100] or in the study of Bhargava and Westmoreland.[101] A shift equaling 4−5 times the orifice diameter has been reported for premixed low-pressure flames. The sampling probes used in these studies for MBMS analyses are not exactly similar with our probe which is smaller, but the principle of sample probe disturbance is generally similar.

dx.doi.org/10.1021/ef301628x | Energy Fuels XXXX, XXX, XXX−XXX

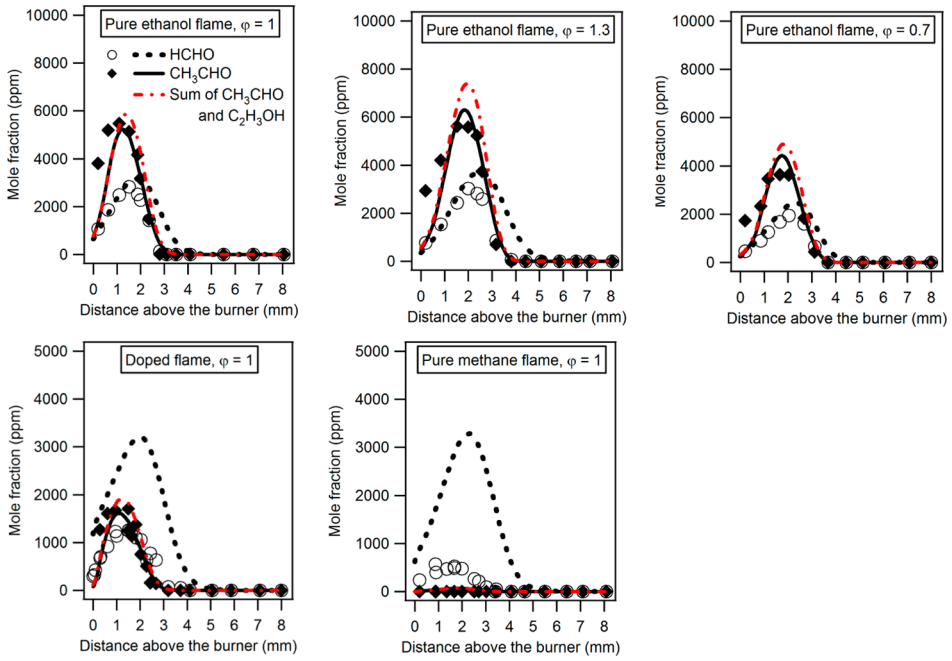

Figure 12. Mole fraction profiles of CH_3CHO and HCHO. Points are experiments and lines simulations: filled diamonds and solid lines, CH_3CHO; open circles and dotted lines, HCHO; dashed−dotted lines, sum of computed mole fractions of CH_3CHO and C_2H_5OH.

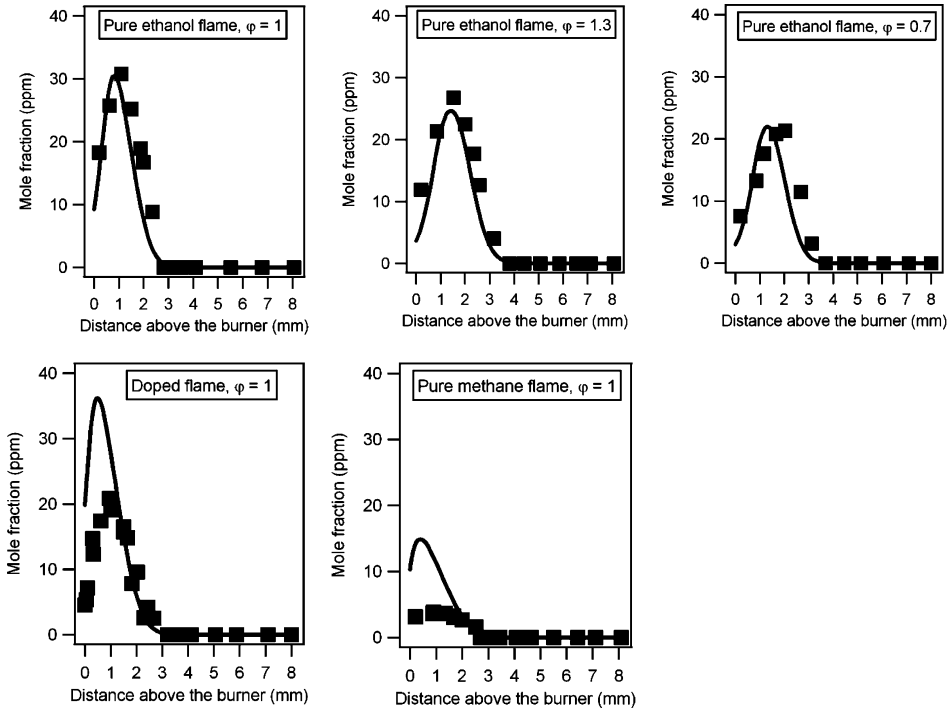

Figure 13. Mole fraction profiles of CH_3OCH_3. Points are experiments and lines simulations: filled squares and solid lines, CH_3OCH_3.

Figures 4−9 show that the model satisfactorily reproduces the consumption of reactants and the formation of the main C_0-C_2 products (nonoxygenated). Only the formation of H_2 (Figure 7) is underestimated by a factor of 1.2 in the reaction zone of the five flames and 1.5 in the burned gases of the rich pure ethanol flame. The formation of C_2H_2 (Figure 9) in the rich pure ethanol flames is underpredicted by a factor of 1.5; that of C_2H_6 (Figure 9) is slightly underpredicted in the ethanol flames and slightly overpredicted in the pure methane flame. Concerning the disagreement described above for H_2, it is probable that the very high diffusivity of H_2 causes an uncertainty in the experimental measurements.

Figures 10 and 11 display the comparison between experimental and simulated data for the C_3 nonoxygenated intermediates. The model reproduces almost satisfactorily the formation of C_3H_6 (Figure 10) and aC_3H_4 (Figure 11). However, the formation of C_3H_8 (Figure 10) is underpredicted by a factor of 2 in the ethanol flames and slightly overpredicted in the pure methane flame. The formation of pC_3H_4 (Figure 11) is underestimated by a factor of 4 in the pure ethanol flames.

dx.doi.org/10.1021/ef301628x | *Energy Fuels* XXXX, XXX, XXX−XXX

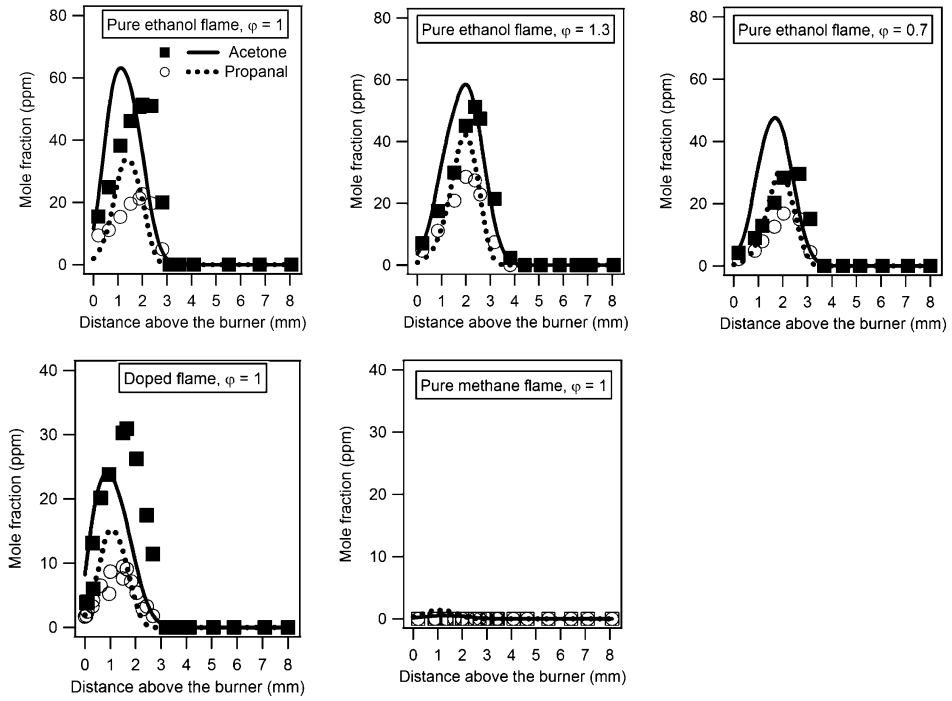

Figure 14. Mole fraction profiles of acetone (CH_3COCH_3) and propanal (C_2H_5CHO). Points are experiments and lines simulations: filled squares and solid lines, CH_3COCH_3; open circles and dotted lines, C_2H_5CHO.

Figures 12−14 display the comparison between experimental and simulated data for the oxygenated intermediates. The model satisfactorily reproduces the formation of CH_3CHO (Figure 12), C_2H_5CHO, and CH_3COCH_3 (Figure 14) in five flames, CH_3OCH_3 (Figure 13) in pure ethanol flames, and HCHO (Figure 12) in pure ethanol flames. However, the formation of HCHO is overpredicted by a factor of 2 in the doped flame and by a factor of 4 in the pure methane flame. The abundance of CH_3 radicals in these two flames largely determines, in the simulation, the formation of formaldehyde via the reaction $CH_3 + O = HCHO + H$. As revealed by the rate-of-production (ROP) analysis, the contribution of this reaction to HCHO formation is about 60% in the pure methane flame, about 43% in the doped flame, and only 10−18% in the pure ethanol flames. The uncertainty on the rate constant of this latter reaction or the underestimation of some competing reaction pathways for methyl radicals could cause the observed disagreement under our conditions for the doped and pure methane flames. The model well predicts the formation of CH_3OCH_3 in the pure ethanol flames but slightly overpredicts it in the doped flame and by a factor of about 2 in the pure methane flame (Figure 13). The ROP analysis shows that CH_3OCH_3 is totally formed through the combination of CH_3 and CH_3O radicals (reaction D1, $CH_3 + CH_3O = CH_3OCH_3$).

Recently, Harper et al.[102] assumed that enols leaving combustion reactors likely tautomerize in the sampling lines to aldehydes before reaching the analytical equipment. The experimental mole fraction profile of acetaldehyde (CH_3CHO) could then be the sum of acetaldehyde and ethenol (vinyl alcohol, C_2H_3OH). However, up until now no experimental evidence supports this assumption. Note that a gas phase conversion of CH_3CHO to C_2H_3OH at low temperature is not compatible with the rate constant calculated in the present work or proposed by Da Silva et al.[76] At the temperature of the sampling line of 423 K, these rate constants calculated by the present work and by Da Silva et al.[76] are quite low (1.07×10^{-15} and 7.68×10^{-17} cm^3 mol^{-1} s^{-1}, respectively). Therefore, the disappearance of C_2H_3OH in the sampling line should result in wall reactions. In the latter case, other reactions such as O−H bond cleavage may be possible and therefore yield products different from CH_3CHO. Nevertheless, a sum of the simulated predictions of CH_3CHO and C_2H_3OH is presented in Figure 12 (dashed−dotted lines), for comparison to the experimental CH_3CHO profiles. This figure shows that the sum of the computed mole fraction profiles of CH_3CHO and C_2H_3OH is slightly higher than that of CH_3CHO, but the agreement with experimental results remains good. The computed profiles of OH, O, H, and CH_3 radicals in these flames are also given in Suporting Information 3.

5.2. Laminar Premixed Flame Result of Xu et al.[20] In order to test our mechanism with another dilution ratio and for the profile of ethenol, the results of Xu et al.,[20] where ethenol (C_2H_3OH) as well as reactive species such as methyl radical (CH_3) and ketene (CH_2CO) were quantified as intermediates, have also been modeled. These results were obtained in a laminar premixed ethanol flame at a pressure of 30 Torr (4.0 kPa) for a stoichiometric mixture, a gas velocity at the burner of 75.4 cm s^{-1} at 473 K, and a dilution of 38.6%. Mass spectrometry with synchrotron photoionization has been used to measure the species formed in this flame with an uncertainty about ±25% for stable species and at least ±40% for the intermediates with an estimated cross section value and radicals. In addition, the uncertainty in the mole fraction of C_2H_6 was about 50% because it was not measured directly. The flame temperature was measured by using a Pt−6%/Rh/Pt−30%Rh thermocouple with a diameter of 100 μm. Figure 15 displays comparisons between the experimental and computed mole fractions of reactants, main products (Figure 15a) and intermediates (Figure 15b−e). These figures show that a globally correct agreement can be observed. The experimental and modeling mole fraction profiles of reactants and main products (Figure 15a) fit quite well, except for CO and H_2 profiles in the reactive zone, and for most main species close to the burner surface. The similar disagreement has also appeared in the results of Xu et al.[20] but without explanation. The disagreement is possibly caused by the effect of the sampling probe.

dx.doi.org/10.1021/ef301628x | Energy Fuels XXXX, XXX, XXX−XXX

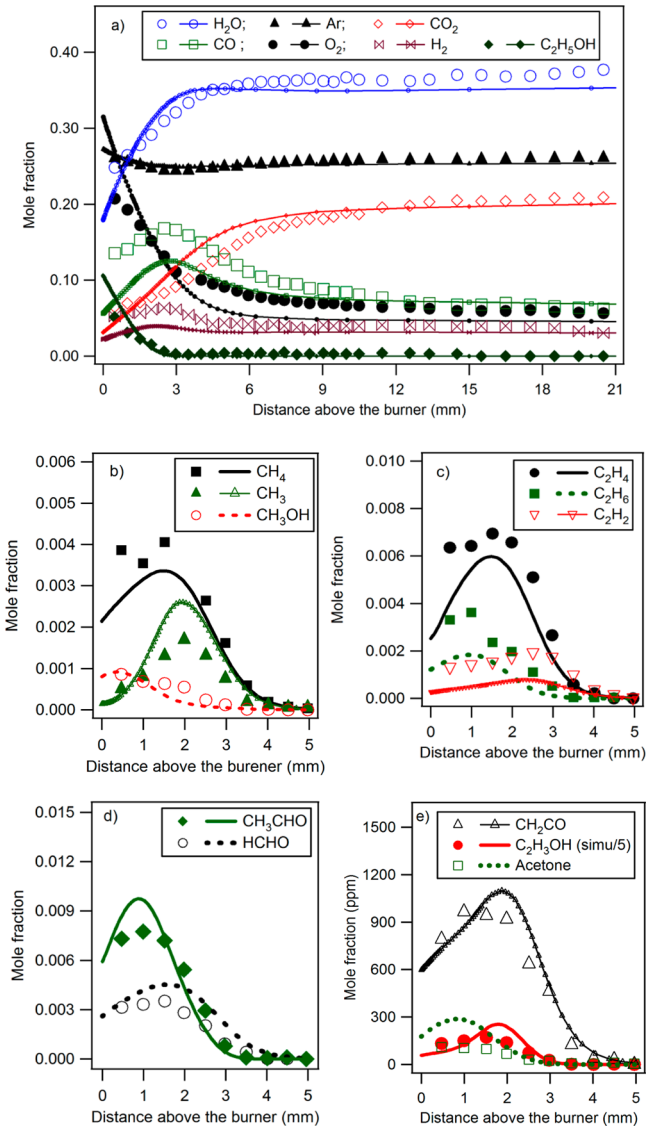

Figure 15. Mole fraction profiles of species in the ethanol flame (φ = 1, dilution = 38.6%): simulation (lines or lines and small symbols); experiment (symbols) from Xu et al.[20].

For C_1 intermediates, the mole fractions of HCHO (Figure 15d), CH_3OH, CH_4 (Figure 15b) are well predicted and that of the methyl radical (CH_3) (Figure 15b) is slightly overpredicted. For C_2 and C_3 intermediates, the formation of C_2H_4 (Figure 15c), CH_3CHO (Figure 15d), and ketene (CH_2CO) (Figure 15e) are satisfactorily reproduced by the model, and that of C_2H_6 and C_2H_2 (Figure 15c) is underestimated by a factor of 1.5−2 and that of acetone and C_2H_3OH (Figure 15e) is also overestimated by a factor of 2 and 5, respectively. The overprediction by a factor of 5 for the C_2H_3OH mole fraction probably simultaneously results from (i) the measurement uncertainty for the mole fraction of C_2H_3OH that is quite reactive, which the photoionization cross section cannot be determined directly with mass spectrometry. Experimental data have previously been obtained for this species under conditions which did not allow individually calculating the measurement uncertainty for this species. (ii) The uncertainties in theoretical calculations for reactions 32, 36, and 42, which are the main reactions of C_2H_3OH formation.[61,70] The flux analysis indicates that C_2H_3OH is mainly formed from the CH_3CHOH radical by β-scission of a C−H bond (reaction 36) (~63% of its formation), by reacting with an H-atom (reaction 42) (~20% of its formation), and from the CH_2CH_2OH radical by β-scission of a C−H bond (reaction 32) (~16% of its formation). No uncertainty limits are given with the theoretical calculations, and no experimental evaluation has previously been done for these reactions. (iii) The uncertainties of rate constants of the H-abstractions (reactions 53−58) from the C_2H_3OH, which are estimated by analogy with the values proposed for acetaldehyde.

5.3. Laminar Burning Velocities Results. The model predictions for laminar burning velocities of ethanol−air flames at atmospheric pressure were compared to data available in studies of Gülder,[32] Egolfopoulos et al.,[31] Liao et al.,[30] Bradley et al.,[33] Konnov et al.,[35] and Glaude et al.[49] (Figure 16). Note that data obtained in the bomb and counterflow burner after 2000 are more reliable since the authors used a nonlinear stretch correction.

The measurements of Gülder[32] and Bradley et al.[33] have been performed using spherical expanding flames in a constant volume bomb. The predicted result, using the empirical relation of Gülder,[32] is also presented for comparison in Figure 16, at a temperature of 453 K, because few experimental data are available under this condition. Egolfopoulos et al.[31] measured the laminar burning velocities of ethanol for initial mixture temperatures between 363 and 453 K using the counterflow twin-flame technique. They reported a linear increase of the burning velocity with temperature and extrapolated their measurements down to 298 K. The study of Liao et al.[30] includes a fitting expression from their experimental data measured in a constant volume combustion bomb with an empirical correlation. The laminar burning velocities presented in Figure 16 for Liao et al.[30] have been calculated using the empirical relation proposed by these authors and have been validated against their experimental data as well as those of Gülder[32] and Egolfopoulos et al.[31] The measurements of Glaude et al.[49] and Konnov et al.[35] have been performed using the heat flux method with a flat flame adiabatic burner.

Figure 16 shows a large range of uncertainties in the laminar burning velocities data taken from measurements as well as from empirical formulas. A globally correct agreement can be observed between predictions with the present model and literature data in Figure 16. The model satisfactorily describes the effect of the equivalence ratios and initial temperatures which considerably influence laminar burning velocities. Note however that at 358 K compared to the experimental data of Glaude et al.[49] and that of Konnov et al.,[35] and at 398 K compared to the data of Glaude et al.,[49] the burning velocities are underestimated for equivalence ratios larger than 1.3. The difference increases with an increasing equivalence ratio. However, under the same conditions (equivalence ratios larger than 1.3 and temperature of 358 K), a quite good agreement can be observed between simulations and the data of Liao et al.[30] and Gülder.[32] At high temperature (453 K), burning velocities are slightly overestimated for equivalence ratios lower than 0.8 compared to the literature data (Gülder,[32] Egolfopoulos et al.,[31] and Liao et al.[30]).

5.4. Comparison with Mechanisms Reported in the Literature. In order to compare our new mechanism with several mechanisms reported in the literature, we present in Figure 17 the experimental (present data) and computed mole fraction profiles of primary intermediate species (C_2H_4, CH_3CHO, HCHO) as well as CH_4 (which can be formed directly from ethanol when CH_3 radical reacts with ethanol) using our mechanism and four mechanisms previously published in the literature: that of Konnov et al.,[68] Marinov,[43] NUIG (De Vies et al.),[95] and the San Diego Mechanism.[96] For reactants and main products, the results show that all these ethanol

dx.doi.org/10.1021/ef301628x | Energy Fuels XXXX, XXX, XXX−XXX

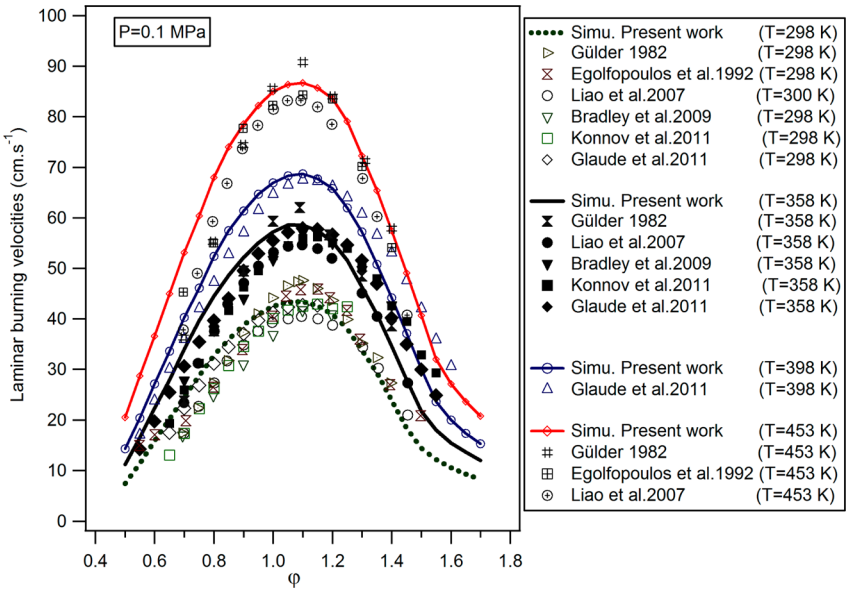

Figure 16. Laminar burning velocities for ethanol−air flames at 0.1 MPa: comparison between modeling (lines and small symbols) and results from Gülder,[32] Egolfopoulos et al.,[31] Liao et al.,[30] Bradley et al.,[33] Konnov et al.,[35] and Glaude et al.[49] (symbols).

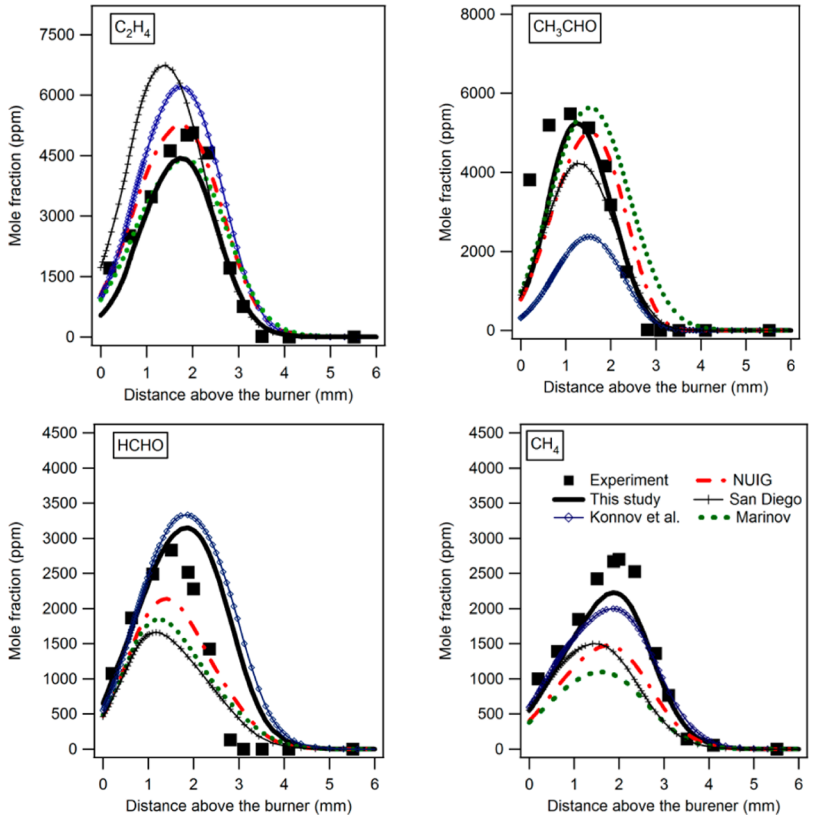

Figure 17. Comparison with the mechanisms reported in the literature: simulation (lines or lines and small symbols) using our mechanism (—) and that of Konnov et al.[68] (blue ◇ with line), Marinov[43] (green ···), NUIG[95] (red — ·), and the San Diego Mechanism[96] (black line with tick lines); experiment (symbols) of present study for the stoichiometric pure ethanol flame. This figure shows only mole fraction profiles of primary products (C_2H_4, CH_3CHO, HCHO) and CH_4.

mechanisms predict reasonably well the experimental profiles (see Figure SI3-3 in the Supporting Information 3). For primary species, the results in Figure 17 show that (1) The formation of ethylene and acetaldehyde is reproduced satisfactorily by the present model and the models of Marinov[43] and NUIG.[95] The formation of acetaldehyde is underestimated by the models of Konnov et al.[68] and that of San Diego,[96] and the formation of ethylene is overestimated by the models of Konnov et al.[68] and San Diego.[96] (2) The present model reproduces quite well the formation of formaldehyde. The model of Konnov et al.[68] slightly overestimates it, and the models of NUIG,[95] Marinov,[43] and San Diego[96] underestimate it. (3) The present model and that of

dx.doi.org/10.1021/ef301628x | Energy Fuels XXXX, XXX, XXX−XXX

Table 4. Branching Ratios of the Three Channels (α_{10}, α_{11}, α_{12}) and the Overall Rate Constant of the Reaction Ethanol + OH → Products + H_2O ($R_{EtOH+OH}$) in the Present Study and in Some Studies of the Literature, at 1200 K

	this work[a]	Xu and Lin[64]	Sivaramakrishnan et al.[110]	NUIG[95]	Marinov[43]	Konnov et al.[68]	San Diego[96]
α_{10}	67.7%	79.3%	92.0%	37.3%	24.8%	32.8%	29.2%
α_{11}	28.3%	15.3%	4.0%	37.8%	16.9%	52.4%	18.2%
α_{12}	4.1%	5.4%	4.0%	24.9%	58.2%	14.9%	52.6%
k_{total} (cm^3 mol^{-1} s^{-1})	1.23×10^{13}	9.22×10^{12}	9.82×10^{12}[b]	6.05×10^{12}	5.42×10^{12}	7.52×10^{12}	4.29×10^{12}

[a]Rate constant of reactions 10 and 11estimated by using the Evans−Polanyi plot proposed by Dean and Bozzelli[63] and that of reaction 12 taken from Xu and Lin[64] (see section 3). [b]Calculated from their adjusted theoretical predictions.

Konnov et al.[68] reproduce quite satisfactorily the formation of methane, while the other models underestimate it.

5.5. Role of Reactions Ethanol + OH in Ethanol Combustion. The reaction C_2H_5OH + OH → Products + H_2O ($R_{EtOH+OH}$) includes three H-abstraction channels of the various sites of ethanol (reactions 10, 11, 12 in Table 3). These reaction channels are important in the consumption pathway of ethanol, and the determination of their rate constants have been the target of several studies.[64,103−112] The overall reaction rate constant k_{total} (sum of k_{10}, k_{11}, and k_{12}) is quite well characterized.[110,111] However, the branching ratios between these three channels (α_{10}, α_{11}, and α_{12}), which play an important role in the subsequent chemistry of ethanol combustion and influence combustion parameters, are poorly established especially at high temperature.[110,111] Among these studies, only Bott and Cohen,[107] Xu and Lin,[64] and Sivaramakrishnan et al.[110] have proposed data in a temperature range above 1000 K (conditions more relevant to combustion). Table 4 shows that a wide variety of branching ratios at 1200 K for the reaction $R_{EtOH+OH}$ has been used in modeling studies of ethanol combustion under high temperature in Konnov et al.,[68] Marinov,[43] NUIG,[95] and the San Diego Mechanism.[96] The trend of the branching ratios used in the present work is similar with those in the theoretical study of Xu and Lin:[64] $\alpha_{10} > \alpha_{11} > \alpha_{12}$. The overall rate constant (k_{total} in Table 4) used in our study is also close to that in the recent studies of Sivaramakrishnan et al.[110] and of Xu and Lin[64] (a factor of about 20−25% of difference, i.e., in the uncertainty range of the theoretical calculation). In order to present the influence of this reaction $R_{EtOH+OH}$ on ethanol combustion, the simulated results using our three channels (R_{10}, R_{11}, and R_{12}) and those of recent studies of Sivaramakrishnan et al.[110] and of Xu and Lin[64] are presented in Figure 18. This figure shows the mole fraction of C_2H_4 (Figure 18a) is well reproduced with the values proposed in the present study, while this species is underpredicted when the values of Xu and Lin[64] or of Sivaramakrishnan et al.[110] are used. The simulated profile of CH_3CHO (Figure 18b) is not affected, with only a small decrease when data of Xu and Lin[64] are used and a very limited increase with those of Sivaramakrishnan et al.[110] The mole fraction profiles of others primary species: HCHO, C_2H_3OH (parts c and d of Figure 18, respectively), and CH_4 (not shown in Figure 18), as well as the laminar burning velocities (Figure 18e) are not significantly influenced by these changes.

6. REACTION PATHWAY ANALYSIS

We discuss here the main flow of consumption of the ethanol under flame conditions with the aim to explain the formation pathways of the observed products. Figure 19 displays the main flow of consumption of ethanol in our stoichiometric pure ethanol flame at a distance of 1.41 mm from the burner corresponding to a simulated temperature of 1137 K and a 64% conversion of ethanol. A large enough conversion has been chosen so that the major ways of consumption of the primary products can be observed. Under these conditions, ethanol is consumed mainly by H-abstraction from the α site (72% of its consumption) to give the α-hydroxyethyl radical (CH_3CHOH). As shown in Figure 1a, in the ethanol molecule, the bond energy of the C−H bond at the α site is the lowest in comparison with that of the C−H bond at the β site and that of the O−H bond. The other channels of consumption of ethanol are the H-abstraction from the β site (23% of its consumption) and the H-abstraction from the hydroxyl group (−OH) (4% of its consumption) to give the β-hydroxyethyl radical (CH_2CH_2OH) and ethoxy radical (CH_3CH_2O), respectively. The contribution of water elimination (reaction 2) is very small (<1% of its consumption).

Subsequently, the α-hydroxyethyl radical reacts mainly by oxidation and by β-scission of the O−H bond to give acetaldehyde (62% of its consumption). Acetaldehyde reacts mainly by H-abstraction from the carbonyl group (−CHO), because of the weakness of the involved C−H bond (see Figure 1b), to give CH_3CO radical which decomposes into methyl radical (CH_3) and CO. Around 22% of α-hydroxyethyl radical gives ethenol (C_2H_3OH) by β-scission of a C−H bond or by reacting with the H-atom. The β-hydroxyethyl radical mainly reacts by β-scission of the C−O bond to give ethylene (78% of its consumption) and around 14% of its consumption gives ethenol by β-scission of a C−H bond. The ethoxy radical is consumed by β-scission of a C−H bond to give acetaldehyde (20% of its consumption) and by β-scission of a C−C bond to give formaldehyde and methyl radicals (66% of its consumption). The combination with the H atom to give back ethanol is a smaller channel of consumption of the α-hydroxyethyl (9% of its consumption), β-hydroxyethyl (7% of its consumption), and ethoxy (14% of its consumption) radicals.

The ethenol, formed from the α-hydroxyethyl or β-hydroxyethyl radicals, is consumed by unimolecular tautomerization (23% of its consumption) to give acetaldehyde, by reaction with H-atom (35% of its consumption) to give ethylene and hydroxyl radical, or by H-abstraction from the hydroxyl group (−OH) (38% of its consumption) to give a CH_2CHO radical.

Propene (C_3H_6) is formed from ethylene (C_2H_4) directly or via the formation of C_2H_3 radicals. Acetylene (C_2H_2) is also formed by decomposition of C_2H_3 radicals. Propyne (pC_3H_4) mainly derives from C_2H_2 directly or via the formation of propargyl radicals (C_3H_3). Allene (aC_3H_4) is the main product of propene reactions via the formation of resonance stabilized allyl radicals (C_3H_5). Ethane (C_2H_6) is produced from a combination of two CH_3 radicals. Propane (C_3H_8) mainly derives from ethane via the combination of C_2H_5 (ethyl) and CH_3 radicals. The source of acetone (CH_3COCH_3) is the combination of CH_3 and CH_3CO radicals (not shown in Figure 19), and the latter is the main product of the H-abstraction from the carbonyl group (−CHO) of acetaldehyde. DME (CH_3OCH_3) is formed from a combination of CH_3O and CH_3 radicals and is mainly consumed by H-abstraction (not shown in Figure 19). Propanal (C_2H_5CHO) is mainly formed by the combinations of CHO and C_2H_5 radicals or

dx.doi.org/10.1021/ef301628x | Energy Fuels XXXX, XXX, XXX−XXX

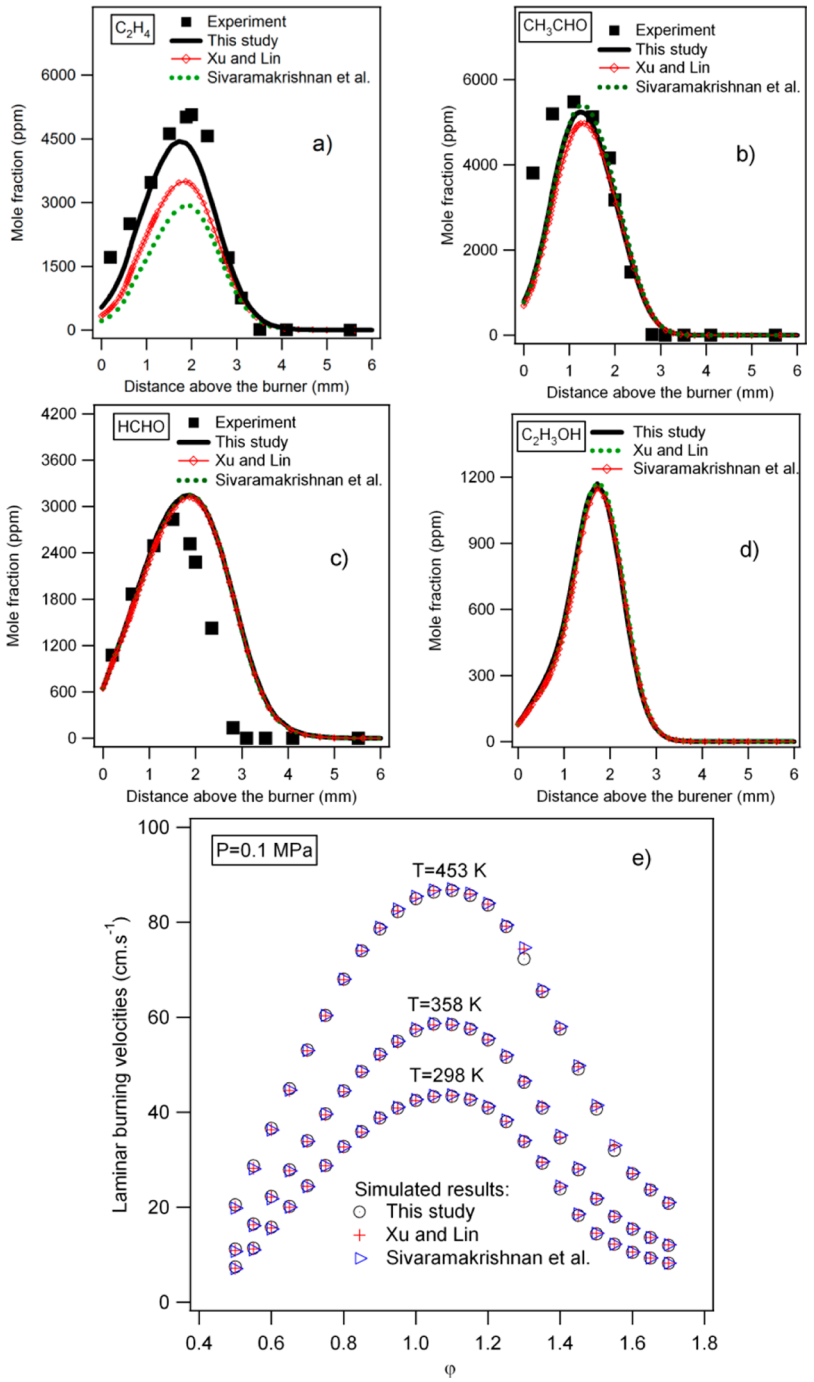

Figure 18. Effect of the reaction C_2H_5OH + OH on the mole fraction profiles of primary species and laminar burning velocities: (a, b, c, and d) experiment (symbols) of present study for the stoichiometric pure ethanol flame; simulation (lines or lines and small symbols) using our three channels of reaction C_2H_5OH + OH, those of Xu and Lin,[64] and of Sivaramakrishnan et al.;[110] (e) laminar burning velocities (only simulated results).

CH_3 and CH_2CHO radicals (not shown in Figure 19) and is mainly consumed by H-abstraction from the carbonyl group (−CHO).

For the other flames (rich, lean, and doped), the same reactions are involved in the consumption of ethanol with small differences in their respective importance. Indeed, when the equivalence ratio decreases, the importance of reactions involving oxygenated reactants, i.e., O atoms, OH radicals, or O_2, is slightly enhanced. Conversely, a higher equivalence ratio slightly increases the importance of the reactions involving species such as H atoms and CH_3 radicals. In the ethanol−methane mixture flame (see its reaction-pathway diagram in Figure 20), CH_4 plays a role as a reactant. CH_4 is mainly consumed by H-abstraction to give CH_3 radicals (100% of its consumption). Therefore, in the ethanol−methane mixture flame, the importance of the reactions with CH_3 radicals is enhanced. For example, in the stoichiometric flames, the mole fraction of C_2H_6 (Figure 9) and C_3H_8 (Figure 10) is increased in the doped flame because C_2H_6 is mainly produced from a combination of two CH_3 radicals, and C_3H_8 derives from ethane via the combination of C_2H_5 and CH_3 radicals.

dx.doi.org/10.1021/ef301628x | Energy Fuels XXXX, XXX, XXX−XXX

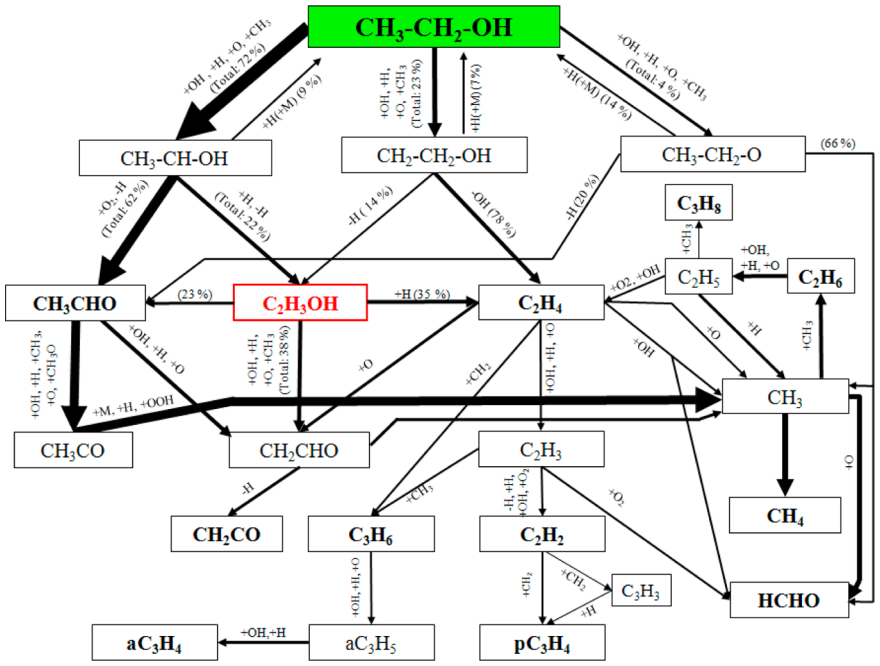

Figure 19. Flow rate analysis for the consumption of ethanol in the stoichiometric ethanol flame (present study) for a distance of 1.41 mm from the burner corresponding to a simulated temperature of 1137 K and a 64% conversion of ethanol. The size of the arrows is proportional to the relative flow rates. In order to simplify the reaction-pathway diagram, final oxidation steps to CO and CO_2 are not shown.

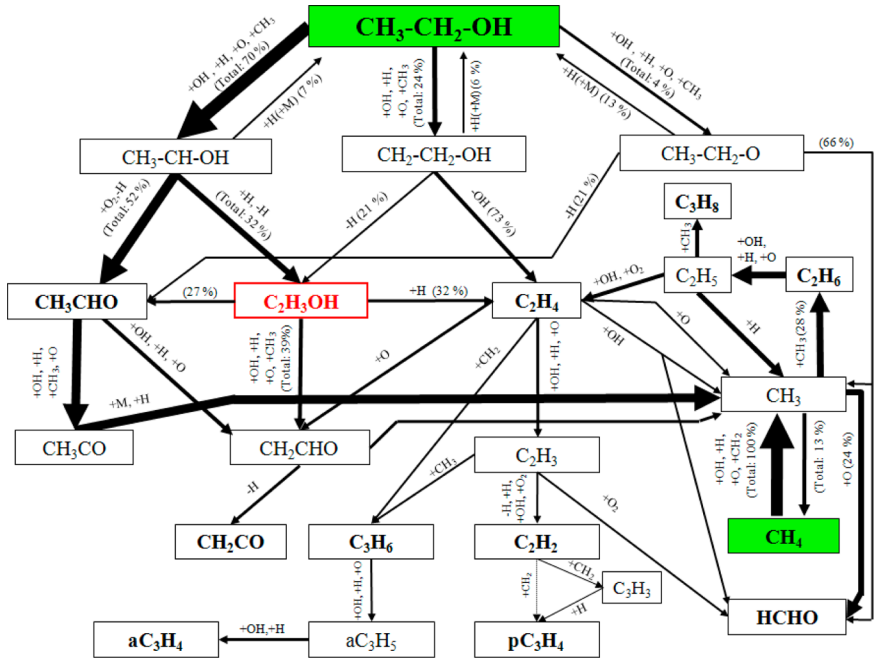

Figure 20. Flow rate analysis for the consumption of ethanol and methane in the ethanol−methane mixture flame for a distance of 1.41 mm from the burner corresponding to a simulated temperature of 1221 K and a 70% conversion of ethanol and a 53% conversion of methane. The size of the arrows is proportional to the relative flow rates. In order to simplify the reaction-pathway diagram, final oxidation steps to CO and CO_2 are not shown.

7. CONCLUSION

This paper presents new experimental results about the structure of five low-pressure laminar premixed flames: a pure flame methane (φ = 1.0), three pure ethanol flames (φ = 0.7, 1.0, 1.3), and a methane flame doped by 30% of ethanol (φ = 1.0). A mechanism is developed to reproduce the combustion of ethanol including the reactions of formation and consumption of ethenol, including the molecular conversion into acetaldehyde which has been studied theoretically.

Profiles of temperature and mole fraction of 20 stable species from C_0 to C_3 have been obtained. Among these 20 species, 5 are oxygenated intermediates. These results show that, for the three pure ethanol flames, the formation of intermediate species is enhanced by increasing the equivalence ratio (except DME). For the three stoichiometric flames, the mole fraction of all intermediates (except C_2H_6) in the pure ethanol flame is the largest, followed by the doped flame, and finally the pure methane flame. That is especially true for toxic aldehydes. Despite its oxygen

dx.doi.org/10.1021/ef301628x | *Energy Fuels* XXXX, XXX, XXX−XXX

content and the close C/O ratio of the stoichiometric flames studied, ethanol produced much more unsaturated hydrocarbons, which are soot precursors, than methane. The structure of the molecule where two carbon atoms are linked favors indeed the formation of C_2 and C_3 compounds in comparison with methane.

A satisfactory agreement has been obtained between experimental results and simulations for most species. The model has also been used with success to simulate results obtained in an ethanol flame by Xu et al.[20] where ethenol was measured and laminar burning velocities results of the literature. The effect of the branching ratios of reaction $C_2H_5OH + OH \rightarrow$ Products + H_2O is also discussed.

Furthermore, this study presents reaction path analysis results for the combustion of ethanol in the stoichiometric ethanol flame. The two significant paths of ethanol consumption are H-abstractions to give acetaldehyde and ethylene via the formations of α- or β-hydroxyethyl radicals, respectively. The present study shows that ethenol is principally formed from α- and β-hydroxyethyl radicals by β-scission of a C−H bond or by reacting with H-atom.

■ ASSOCIATED CONTENT

Supporting Information

(Supporting Information 1) Complete mechanism of the oxidation of ethanol and the transport data is given under CHEMKIN format; (Supporting Information 2) experimental data are given in tabular form; and (Supporting Information 3) scheme of the end of sampling probe, computed profiles of OH, O, H, HO_2, and CH_3 radicals in these five flames, and comparison between the experimental and computed mole fraction profiles of reactants and main products, using our mechanism and four mechanisms previously published in the literature (Konnov et al.,[68] Marinov,[43] NUIG,[95] and the San Diego Mechanism[96]). This material is available free of charge via the Internet at http://pubs.acs.org.

■ AUTHOR INFORMATION

Corresponding Author

*Phone: +33383175125. Fax: +33383378120. E-mail: frederique.battin-leclerc@univ-lorraine.fr.

Notes

The authors declare no competing financial interest.

■ ACKNOWLEDGMENTS

This work was funded by the European Commission through the "Clean ICE" Advanced Research Grant of the European Research Council. This work was granted access to the HPC resources of CINES under Allocation c2012086686 made by GENCI (Grand Equipement National de Calcul Intensif). The authors wish to thank Professor Edward Blurock for his help in checking the English in the manuscript.

■ REFERENCES

(1) Román-Leshkov, Y.; Barrett, C. J.; Liu, Z. Y.; Dumesic, J. A. *Nature* **2007**, *447*, 982−985.
(2) Gouli, S.; Lois, E.; Stournas, S. *Energy Fuels* **1998**, *12*, 918−924.
(3) Thewes, M.; Muether, M.; Pischinger, S.; Budde, M.; Brunn, A.; Sehr, A.; Adomeit, P.; Klankermayer, J. *Energy Fuels* **2011**, *25*, 5549−5561.
(4) Yang, W.; Sen, A. *ChemSusChem* **2010**, *3*, 597−603.
(5) Ballerini, D. *Les Biocarburants: Etat des Lieux, Perspectives et Enjeux du Développement*; Editions TECHNIP: Paris, France, 2006.
(6) Agarwal, A. K. *Prog. Energy Combust. Sci.* **2007**, *33*, 233−271.
(7) He, J.; Zhang, W. *Appl. Energy* **2011**, *88*, 1224−1232.
(8) Singh, A.; Nigam, P. S.; Murphy, J. D. *Bioresour. Technol.* **2011**, *102*, 10−16.
(9) Kohse-Höinghaus, K.; Oßwald, P.; Cool, T. A.; Kasper, T.; Hansen, N.; Qi, F.; Westbrook, C. K.; Westmoreland, P. R. *Angew. Chem., Int. Ed.* **2010**, *49*, 3572−3597.
(10) Balat, M.; Balat, H.; Öz, C. *Prog. Energy Combust. Sci.* **2008**, *34*, 551−573.
(11) Service, R. F. *Science* **2007**, *315*, 1488−1491.
(12) Brown, J.; Tipper, C. F. H. *Proc. R. Soc. London A* **1969**, *312*, 399−415.
(13) Haas, F. M.; Chaos, M.; Dryer, F. L. *Combust. Flame* **2009**, *156*, 2346−2350.
(14) Cooke, D. F.; Dodson, M. G.; Williams, A. *Combust. Flame* **1971**, *16*, 233−236.
(15) Tsang, W. *Int. J. Chem. Kinet.* **1976**, *8*, 173−192.
(16) Lee, B. C.; Vranckx, S.; Heufer, K. A.; Khomik, S. V.; Uygun, Y.; Olivier, H.; Fernandes, R. X. *Z. Phys. Chem.* **2012**, *226*, 1−27.
(17) Smith, S. R.; Gordon, A. S. *J. Phys. Chem.* **1956**, *60*, 1059−1062.
(18) Leplat, N.; Dagaut, P.; Togbé, C.; Vandooren, J. *Combust. Flame* **2011**, *158*, 705−725.
(19) Leplat, N.; Seydi, A.; Vandooren, J. *Combust. Sci. Technol.* **2008**, *180*, 519−532.
(20) Xu, H.; Yao, C.; Yuan, T.; Zhang, K.; Guo, H. *Combust. Flame* **2011**, *158*, 1673−1681.
(21) Kasper, T. S.; Oßwald, P.; Kamphus, M.; Kohse-Höinghaus, K. *Combust. Flame* **2007**, *150*, 220−231.
(22) Wang, J.; Struckmeier, U.; Yang, B.; Cool, T. A.; Osswald, P.; Kohse-Höinghaus, K.; Kasper, T.; Hansen, N.; Westmoreland, P. R. *J. Phys. Chem. A* **2008**, *112*, 9255.
(23) Dagaut, P.; Togbe, C. *Energy Fuels* **2008**, *22*, 3499−3505.
(24) Frassoldati, A.; Cuoci, A.; Faravelli, T.; Ranzi, E. *Combust. Sci. Technol.* **2010**, *182*, 653−667.
(25) Frassoldati, A.; Faravelli, T.; Ranzi, E.; Kohse-Höinghaus, K.; Westmoreland, P. R. *Combust. Flame* **2011**, *158*, 1264−1276.
(26) Gerasimov, I. E.; Knyazkov, D. A.; Yakimov, S. A.; Bolshova, T. A.; Shmakov, A. G.; Korobeinichev, O. P. *Combust. Flame* **2012**, *159*, 1840−1850.
(27) Farrell, J. T.; Johnston, J.; Androulakis, I. P. SAE Technical Paper, Paper No. 2004-01-2936, 2004, DOI: 10.4271/2004-01-2936.
(28) Jerzembeck, S.; Peters, N.; Pepiot-Desjardins, P.; Pitsch, H. *Combust. Flame* **2009**, *156*, 292−301.
(29) Marshall, S. P.; Taylor, S.; Stone, C. R.; Davies, T. J.; Craknell, R. F. *Combust. Flame* **2011**, *158*, 1920−1932.
(30) Liao, S. Y.; Jiang, D. M.; Huang, Z. H.; Zeng, K.; Cheng, Q. *Appl. Therm. Eng.* **2007**, *27*, 374−380.
(31) Egolfopoulos, F. N.; Du, D. X.; Law, C. K. *Proc. Combust. Inst.* **1992**, *24*, 833−841.
(32) Gülder, O. L. *Proc. Combust. Inst.* **1982**, *19*, 275−281.
(33) Bradley, D.; Lawes, M.; Mansour, M. *Combust. Flame* **2009**, *156*, 1462−1470.
(34) Veloo, P.; Wang, Y.; Egolfopoulos, F.; Westbrook, C. *Combust. Flame* **2010**, *157*, 1989−2004.
(35) Konnov, A. A.; Meuwissen, R.; De Goey, L. *Proc. Combust. Inst.* **2011**, *33*, 1011−1019.
(36) Eisazadeh-Far, K.; Moghaddas, A.; Al-Mulki, J.; Metghalchi, H. *Proc. Combust. Inst.* **2011**, *33*, 1021−1027.
(37) Broustail, G.; Seers, P.; Halter, F.; Moréac, G.; Mounaim-Rousselle, C. *Fuel* **2011**, *90*, 1−6.
(38) Van Lipzig, J. V.; Nilsson, E.; Goey, L. D.; Konnov, A. *Fuel* **2011**, *90*, 2773−2781.
(39) Natarajan, K.; Bhaskaran, K. A. In *Shock Tubes and Waves Proceeidngs of the 13th International Symposium on Shock Tubes and Waves*; July 6−9, 1981, Niagara Falls, NY, State University of New York Press: Albany, NY, 1982; pp 834−842.
(40) Dunphy, M. P.; Patterson, P. M.; Simmie, J. M. J. *Chem. Soc. Faraday Trans.* **1991**, *87*, 2549−2559.
(41) Norton, T. S.; Dryer, F. L. *Int. J. Chem. Kinet.* **1992**, *24*, 319−344.
(42) Dagaut, P.; Boettner, J. C.; Cathonnet, M. *J. Chim. Phys.* **1992**, *89*, 867−884.

(43) Marinov, N. M. *Int. J. Chem. Kinet.* **1999**, *31*, 183−220.
(44) Saxena, P.; Williams, F. A. *Proc. Combust. Inst.* **2007**, *31*, 1149−1156.
(45) Li, J.; Kazakov, A.; Chaos, M.; Dryer F. L. *5th U.S. Combustion Meeting*, San Diego, CA, 2007.
(46) Cancino, L. R.; Fikri, M.; Oliveira, A. A. M.; Schulz, C. *Energy Fuels* **2010**, *24*, 2830−2840.
(47) Zhao, Z.; Chaos, M.; Kazakov, A.; Dryer, F. L. *Int. J. Chem. Kinet.* **2008**, *40*, 1−18.
(48) Taatjes, C. A.; Hansen, N.; Miller, J. A.; Cool, T. A.; Wang, J.; Westmoreland, P. R.; Law, M. E.; Kasper, T.; Kohse-Höinghaus, K. *J. Phys. Chem. A* **2006**, *110*, 3254−3260.
(49) Glaude, P. A.; Herbinet, O.; Dirrenberger, P.; Bounaceur, R.; Le Gall, H.; Battin-Leclerc, F.; Pires da Cruz, A.; Konnov, A. A. *European Combustion Meeting*, Cardiff, Wales, U.K., June 29−July 1, 2011.
(50) Pousse, E.; Glaude, P. A.; Fournet, R.; Battin-Leclerc, F. *Combust. Flame* **2009**, *156*, 954−974.
(51) Kint, J. H. *Combust. Flame* **1970**, *14*, 279−281.
(52) Bonne, U.; Grewer, T.; Wagner, A. A. M. *Z. Phys. Chem.* **1960**, *26*, 93−110.
(53) Fournet, R.; Bauge, J. C.; Battin-Leclerc, F. *Int. J. Chem. Kinet.* **1999**, *31*, 361−379.
(54) Belmekki, N.; Glaude, P. A.; Da Costa, I.; Fournet, R.; Battin-Leclerc, F. *Int. J. Chem. Kinet.* **2002**, *34*, 172−183.
(55) Gueniche, H. A.; Biet, J.; Glaude, P. A.; Fournet, R.; Battin-Leclerc, F. *Fuel* **2009**, *88*, 1388−1393.
(56) Baulch, D. L.; Bowman, C. T.; Cobos, C. J.; Cox, R. A.; Just, T.; Kerr, J. A.; Pilling, M. J.; Stocker, D.; Troe, J.; Tsang, W.; Walker, R. W.; Warnatz, J. *J. Phys. Chem. Ref. Data* **2005**, *34*, 757−1397.
(57) Tsang, W.; Hampson, R. F. *J. Phys. Chem. Ref. Data* **1986**, *15*, 1087−1279.
(58) Troe, J. *Ber. Buns. Phys. Chem* **1974**, *78*, 478−485.
(59) Kee, R. J.; Rupley, F. M.; Miller, J. A. *Sandia Laboratories Report S 89-8009B*, 1993.
(60) Tsang, W. *Int. J. Chem. Kinet.* **2004**, *36*, 456−465.
(61) Xu, Z. F.; Xu, K.; Lin, M. C. *J. Phys. Chem. A* **2011**, *115*, 3509−3522.
(62) Ingham, T.; Walker, R. W.; Woolford, R. E. *Proc. Combust. Instit.* **1994**, *25*, 767−774.
(63) Dean, A. M.; Bozzelli, J. W. *Combustion Chemistry of Nitrogen, in Gas-phase Combustion Chemistry*; Gardiner, W. C., Ed., Springer-Verlag: New York, 2000.
(64) Xu, S.; Lin, M. C. *Proc. Combust. Instit.* **2007**, *31*, 159−166.
(65) Wu, C. W.; Lee, Y. P.; Xu, S.; Lin, M. C. *J. Phys. Chem. A* **2007**, *111*, 6693−6703.
(66) Park, J.; Xu, Z. F.; Lin, M. C. *J. Chem. Phys.* **2003**, *118*, 9990−9996.
(67) Xu, Z. F.; Park, J.; Lin, M. C. *J. Chem. Phys.* **2004**, *120*, 6593−6599.
(68) Konnov, A. A.; Barnes, F. J.; Bromly, J. H.; Zhu, J. N.; Zhang, D. K. *Combust. Flame* **2005**, *141*, 191−199.
(69) Grana, R.; Frassoldati, A.; Faravelli, T.; Niemann, U.; Ranzi, E.; Seiser, R.; Cattolica, R.; Seshadri, K. *Combust. Flame* **2010**, *157*, 2137−2154.
(70) Xu, Z. F.; Xu, K.; Lin, M. C. *ChemPhysChem* **2009**, *10*, 972−982.
(71) Da Silva, G.; Bozzelli, J. W.; Liang, L.; Farrell, J. T. *J. Phys. Chem. A* **2009**, *113*, 8923−8933.
(72) Taatjes, C. A.; Hansen, N.; McIlroy, A.; Miller, J. A.; Senosiain, J. P.; Klippenstein, S. J.; Qi, F.; Sheng, L.; Zhang, Y.; Cool, T. A.; et al. *Science* **2005**, *308*, 1887−1889.
(73) Cool, T. A.; Nakajima, K.; Mostefaoui, T. A.; Qi, F.; McIlroy, A.; Westmoreland, P. R.; Law, M. E.; Poisson, L.; Peterka, D. S.; Ahmed, M. *J. Chem. Phys.* **2003**, *119*, 8356−8365.
(74) Buda, F.; Bounaceur, R.; Warth, V.; Glaude, P. A.; Fournet, R.; Battin-Leclerc, F. *Combust. Flame* **2005**, *142*, 170−186.
(75) Da Silva, G.; Bozzelli, J. W. *J. Phys. Chem. A* **2006**, *110*, 13058−13067.
(76) Da Silva, G.; Kim, C. H.; Bozzelli, J. W. *J. Phys. Chem. A* **2006**, *110*, 7925−7934.
(77) Huynh, L. K.; Zhang, H. R.; Zhang, S.; Eddings, E.; Sarofim, A.; Law, M. E.; Westmoreland, P. R.; Truong, T. N. *J. Phys. Chem. A* **2009**, *113*, 3177−3185.
(78) Warnatz, J. Rate Coefficients in the C/H/O System. In *Combustion Chemistry*; Gardiner, W. C., Jr., Ed.; Springer-Verlag: New York, 1984.
(79) Wilk, R. D.; Cernansky, N. P.; Pitz, W. J.; Westbrook, C. K. *Combust. Flame* **1989**, *77*, 145−170.
(80) Hippler, H.; Viskolcz, B. *Phys. Chem. Chem. Phys.* **2000**, *2*, 3591−3596.
(81) Montgomery, J. A.; Frisch, M. J.; Ochterski, J. W.; Petersson, G. A. *J. Chem. Phys.* **1999**, *110*, 2822−2827.
(82) Frisch, M. J.; Trucks, G. W.; Schlegel, H. B.; Scuseria, G. E.; Robb, M. A.; Cheeseman, J. R.; Montgomery, J. J. A.; Vreven, T.; Kudin, K. N.; Burant, J. C. et al. *Gaussian 03*; Gaussian Inc.: Pittsburgh, PA, 2003.
(83) Sirjean, B.; Glaude, P. A.; Ruiz-Lopez, M. F.; Fournet, R. *J. Phys. Chem. A* **2006**, *110*, 12693−12704.
(84) Teixeira-Dias, J. J. C.; Furlani, T. R.; Shores, K. S.; Garvey, J. F. *Phys. Chem. Chem. Phys.* **2003**, *5*, 5063−5069.
(85) Mokrushin, V.; Tsang, W. *Chemrate*, v.1.5.8; Mokrushin Software: Gaithersburg, MD, 2009.
(86) Eckart, C. *Phys. Rev.* **1930**, *35*, 1303.
(87) Pitzer, K. S.; Gwinn, W. D. *J. Chem. Phys.* **1942**, *10*, 428.
(88) Chong, C. T.; Hochgreb, S. *Combust. Flame* **2011**, *158*, 490−500.
(89) Xu, F.; Lin, K. C.; Faeth, G. M. *Combust. Flame* **1998**, *115*, 195−209.
(90) Sivaramakrishnan, R.; Michael, J. V.; Klippenstein, S. J. *J. Phys. Chem. A* **2010**, *114*, 755−764.
(91) Cavanagh, J.; Cox, R. A. *Combust. Flame* **1990**, *82*, 15−39.
(92) Scherzer, K.; Loser, U.; Stiller, W. *Z. Chem.* **1987**, *27*, 300−301.
(93) Hohlein, G.; Freeman, G. R. *J. Am. Chem. Soc.* **1970**, *92*, 6118−6125.
(94) Erlenmeyer, E. *Chem. Ber.* **1880**, *13*, 305−310.
(95) De Vies, J.; Lowry, W. B.; Serinyel, Z.; Curran, H. J.; Petersen, E. L. *Fuel* **2011**, *90*, 331−338, http://c3.nuigalway.ie/mechanisms.html, Available at http://c3.nuigalway.ie/mechanisms.html.
(96) Complete San Diego Mechanism of the Combustion Research Group in Department of Mechanical and Aerospace Engineering, University of California at San Diego. Version 2011-11-22. Available at http://web.eng.ucsd.edu/mae/groups/combustion/mechanism.html
(97) Blank, B.; Fischer, H. *Helv. Chim. Acta* **1973**, *56*, 506−510.
(98) Saito, S. *Chem. Phys. Lett.* **1976**, *42*, 399−623.
(99) Hartlieb, A. T.; Atakan, B.; Kohse-Höinghaus, K. *Combust. Flame* **2000**, *121*, 610−624.
(100) Struckmeier, U.; Oßwald, P.; Kasper, T.; Böling, L.; Heusing, M.; Köhler, M.; Brockhinke, A.; Kohse-Höinghaus, K. *Z. Phys. Chem.* **2009**, *223*, 503−537.
(101) Bhargava, A.; Westmoreland, P. R. *Combust. Flame* **1998**, *113*, 333−347.
(102) Harper, M. R.; Van Geem, K. M.; Pyl, S. P.; Marin, G. B.; Green, W. H. *Combust. Flame* **2011**, *158*, 16−41.
(103) Meier, U.; Grotheer, H. H.; Riekert, G.; Just, T. *Chem. Phys. Lett.* **1985**, *115*, 221−225.
(104) Meier, U.; Grotheer, H. H.; Riekert, G.; Just, T. *Chem. Phys. Lett.* **1987**, *133*, 162−164.
(105) Wallington, T. J.; Kurylo, M. J. *Int. J. Chem. Kinet.* **1987**, *19*, 1015−1023.
(106) Hess, W. P.; Tully, F. P. *Chem. Phys. Lett.* **1988**, *152*, 183−189.
(107) Bott, J. F.; Cohen, N. *Int. J. Chem. Kinet.* **1991**, *23*, 1075−1094.
(108) Jimenez, E.; Gilles, M. K.; Ravishankara, A. R. *J. Photochem. Photobiol. A* **2003**, *157*, 237−245.
(109) Dillon, T. J.; Holscher, D.; Sivakumaran, V.; Horowitz, A.; Crowley, J. N. *Phys. Chem. Chem. Phys.* **2005**, *7*, 349−355.
(110) Sivaramakrishnan, R.; Su, M. C.; Michael, J. V.; Klippenstein, S. J.; Harding, L. B.; Ruscic, B. *J. Phys. Chem. A* **2010**, *114*, 9425−9439.
(111) Carr, S. A.; Blitz, M. A.; Seakins, P. W. *J. Phys. Chem. A* **2011**, *115*, 3335−3345.
(112) Galano, A.; Alvarez-Idaboy, J. R.; Bravo-Perez, G.; Ruiz-Santoyo, M. E. *Phys. Chem. Chem. Phys.* **2002**, *4*, 4648−4662.